DESIGN OF CAPACITIVE MICROMACHINED ULTRASONIC TRANSDUCER FOR UNDERWATER ACOUSTIC IMAGING

A Dissertation Submitted in partial fulfilment of the requirements for the award of the degree of

Masters of Engineering

In

Electronics and Communication Engineering

Submitted by

Vinod Bhonsle

Roll No. : 801361030

Under the guidance of

Dr. Anil Arora

Assistant Professor, ECED

Thapar University, Patiala

ELECTRONICS AND COMMUNICATION ENGINEERING DEPARTMENT

THAPAR UNIVERSITY

(Established under the section 3 of UGC Act, 1956)

PATIALA – 147004 (PUNJAB)

CERTIFICATE

I, Vinod Bhonsle, hereby declare that the work which is being presented in the dissertation entitled, **"DESIGN OF CAPACITIVE MICROMACHINED ULTRA-SONIC TRANSDUCER FOR UNDERWATER ACOUSTIC IMAGING"** by me in partial fulfillment of the requirement for the award of degree of M.E in Electronics and Communication submitted in Electronics and Communication Engineering Department of Thapar University, Patiala is an authentic record of my own work carried out under the supervision of **Dr. Anil Arora**, Assistant Professor, ECED. The matter presented in this dissertation has not been submitted in any other University/Institute for the award of degree.

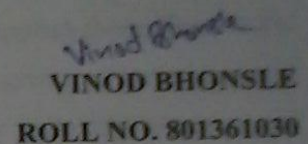

Date: 13/7/15

VINOD BHONSLE
ROLL NO. 801361030

It is certified that the above statement made by the student is correct to the best of my knowledge and belief.

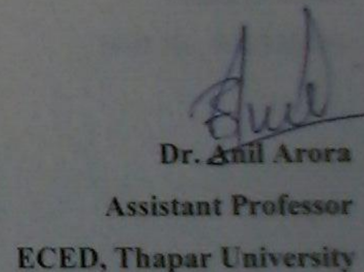

Date: 13/7/15

Dr. Anil Arora
Assistant Professor
ECED, Thapar University

Countersigned By:-

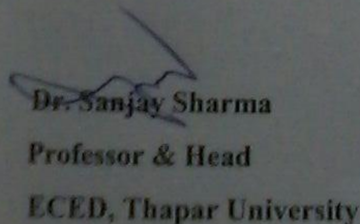

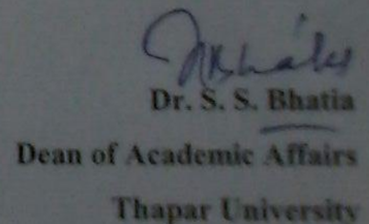

Dr. Sanjay Sharma
Professor & Head
ECED, Thapar University

Dr. S. S. Bhatia
Dean of Academic Affairs
Thapar University

ACKNOWLEDGEMENT

I would like to express my gratitude to **Dr. Anil Arora,** Assistant Professor, electronics and communication engineering department, Thapar University, Patiala for his patience guidance and support throughout this report work. I am truly very fortunate to have the opportunity to work with him. He has provided help in technical writing, presentation style and I found this guidance to be extremely valuable.

I am highly grateful to **Dr. Sanjay Sharma**, Head, Department of Electronics and Communication, Thapar University, Patiala, for providing this opportunity to carry out the present work.

I also express my gratitude to **Dr. Amit Kumar Kohli,** P.G. Coordinator, Electronics and Communication Engineering Department, the entire faculty and staff members of Electronics and Communication Engineering department for their unyielding encouragement.

I am greatly indebted to all my friends, who have graciously applied themselves to the task of helping me with ample moral support and valuable suggestion. Finally, I would like to extend my gratitude to all those persons who directly or indirectly helped me in process and contributed toward this work.

Vinod Bhonsle

Roll No. 801361030

ABSTRACT

We introduce Capacitive Micromachined Ultrasonic Transducer (CMUT) for underwater acoustic imaging in order to obtain the high resolution images. CMUT is used because of its several advantages like higher performance, low motional impedance and high quality factor, high bandwidth, less losses. The CMUT consists of a membrane. When AC voltage superimposed with DC voltage is applied across metalized membrane and substrate, ultrasonic waves are produced. The membrane is attracted towards the bulk by the electrostatic force and induced stress within the membrane resists the attraction. If the biased membrane is exposed to ultrasound, a current is generated due to the capacitance change under constant bias voltage. The amplitude of this current is a function of the frequency of the incident wave, the bias voltage, and the capacitance of the device. In this report comparative study of CMUT has been done. Objectives have been drawn from the observations and gaps. Simulation results have been achieved using COMSOL multiphysics.

TABLE OF CONTENTS

CONTENTS **Page No.**

CERTIFICATE	i
ACKNOWLEDGMENT	ii
ABSTRACT	iii
CONTENTS	iv
LIST OF ACRONYMS	vi
LIST OF FIGURES	viii
LIST OF TABLES	x
CHAPTER-1 INTRODUCTION	**1**
1.1 Background	1
1.2 Introduction to CMUT (Capacitive Micromachined Ultrasonic Transducer)	2
1.3 Importance of CMUT	3
1.4 Applications of CMUT	4
1.5 Gaps in study of CMUT	4
1.6 Thesis significance	4
1.7 Thesis outline	5
CHAPTER-2 LITERATURE SURVEY	**6**
CHAPTER-3 OPERATING PRINCIPLE OF CMUT	**14**
3.1 CMUT operation	15
3.2 Equivalent circuit of CMUT	17
3.3 Important parameters in CMUT	22

3.3.1 Pull in voltage 22

3.3.2 Resonant frequency 24

CHAPTER-4 DESCRIPTION OF COMSOL SOFTWARE 25

4.1 COMSOL Multiphysics 25

4.2 Methodology of working on COMSOL 25

4.3 Brief description of all modules in COMSOL 27

4.4 Coupling of physics 32

CHAPTER-5 FABRICATION STEPS OF CMUT 35

5.1 Fabrication process flow 36

CHAPTER-6 RESULTS AND DISCUSSIONS 40

6.1 Shape and material of membrane 40

6.1.1 Shape of membrane 40

6.1.2 Membrane materials 40

6.2 Frequency analysis of membrane designs and simulation results 41

6.2.1 Simulation results for three membranes 42

6.2.2 Frequency analysis of different membranes 44

6.3 Deflection of membranes under DC bias voltage 46

CHAPTER-7 CONCLUSION, RECOMMENDATIONS AND FUTURE SCOPE 56

REFERENCES 58

LIST OF PUBLICATIONS 64

LIST OF ACRONYMS

AR	Air ratio of holes
BW	Bandwidth
BEM	Boundary Element Method
CMUT	Capacitive Micromachined Ultrasonic Transducer
CRP	Carbon-fiber reinforced polymer
DAS	Data Acquisition System
EM	Electromagnetic
ETR	Electromechanical Transformer Ratio
FEA	Finite Element Analysis
HIFU	High Intensity Focused Ultrasound
HMI	Human Machine Interface
IC	Integrated Circuit
IVUS	Intravascular Ultrasound
LPA	Linear Phased Arrays
LPCVD	Low Pressure Chemical Vapor Deposition
MEMS	Micro-electromechanical Systems
MUMPS	Multi-user Micro-electromechanical Systems (MEMS) Processes
MUT	Micromachined Ultrasonic Transducers
NDT	Non-destructive Testing
ODT	Optical Detection Technique
PDE	Partial Differential Equations
PECVD	Plasma-Enhanced Chemical Vapor Deposition
PR	Perforation Ratio
RCA	Radio Corporation of America
RIE	Reactive Ion Etch
SMCUI	Surface Micromachined Capacitive Ultrasonic Immersion
SL	Sacrificial layer
SNR	Signal-to-Noise Ratio

TMAH	Tetra-Methyl Ammonium Hydroxide
VUI	Volumetric Ultrasound Imaging

LIST OF FIGURES

No.	TITLE	PAGE No.
1.1	Basic block diagram of MEMS	2
3.1	Schematic cross section of a 1-D CMUT cell	14
3.2	CMUT cells connected in parallel	14
3.3	Top view of CMUT cell	14
3.4	Working principle of CMUT	15
3.5	First order lumped electromechanical model of transducer element	17
3.6	Equivalent circuit of CMUT	21
3.7	Cross sectional view of a collapsed mode CMUT	22
4.1	COMSOL Multiphysics window	26
4.2	Setup study type in COMSOL Multiphysics	27
4.3	Coupling of physics in COMSOL	32
5.1	Low temperature process flow illustration for immersion CMUT	37
6.1	Simulated circular membrane	42
6.2	Simulated square membrane	43
6.3	Simulated hexagonal membrane	44
6.4	Frequency versus deflection graph of three membranes	44
6.5	Frequency versus deflection graph of hexagonal membrane using silicon, silicon nitride and polysilicon	45
6.6	Total displacement versus voltage graph when no load is applied on transducer	46
6.7	Total displacement versus voltage graph under the effect of 1 atm pressure	47
6.8	Total displacement versus voltage graph under the effect of water	48
6.9	Simulated Capacitive Micromachined Ultrasonic Transducer	49

6.10	Transient response of CMUT at 2 MHz	50
6.11	Eigen frequency versus DC bias	52
6.12	Simulated hexagonal CMUT	53
6.13	Effect of top electrode	54
6.14	Effect of area on top electrode	54
6.15	Change in capacitance	55
7.1	Circular close packing	56
7.2	Hexagonal close packing	56
7.3	Square close packing	56

LIST OF TABLES

No.	TITLE	PAGE No.
6.1	Area utilization of various shapes	40
6.2	Mechanical properties of materials	41
6.3	Table of depth versus pressure	47
6.4	List of parameters of CMUT	48
6.5	Table of simulated data for CMUT	51
6.6	Parameters for hexagonal CMUT	53

CHAPTER 1

INTRODUCTION

1.1 BACKGROUND

In 21st century, there is growing interest to minimize the size and the power consumption of any electronic device. There are many technologies introduced but the most optimistic technology is identified as MEMS.

MEMS are micro-scale devices which combine electrical and movable mechanical components. MEMS devices utilize principles of physics and chemistry like force, temperature, electromagnetic reaction and movement to sense any variations in the system. The electronic section processes the information from the sensing unit by converting the information into an electrical signal and responding to that change. These kinds of MEMS devices are categorized as "sensors".

MEMS is combination of three basic blocks named as sensor, processor and actuator as shown in fig. 1.1 [1]. Sensor or micro sensor is first block which senses the measurand or input signal. Most of time input is probably non-electrical signal which converts into electrical signal. Non electrical signals may be different possible signals like, thermal, radiation, mechanical, magnetic, optical or bio (chemical). All signals must be converted into electrical signal by sensor using available possible methods of conversion. Processor is next to sensor block which gets electrical signal from sensor. It does some mathematical or logical operations (decision making operations) on signal. Processor has electrical signal as input and output. The final building block is actuator which has electrical signal from processor as input and generally non - electrical signal as output. It does exactly opposite conversion of signal that is discussed in sensor. It converts electrical signal into non – electrical signals like, thermal, radiation, mechanical, magnetic, optical or bio (chemical). Actuator actually responds to environment (e.g. pumping, filtering, positioning, regulating and moving) based on intended designed instruction [1].

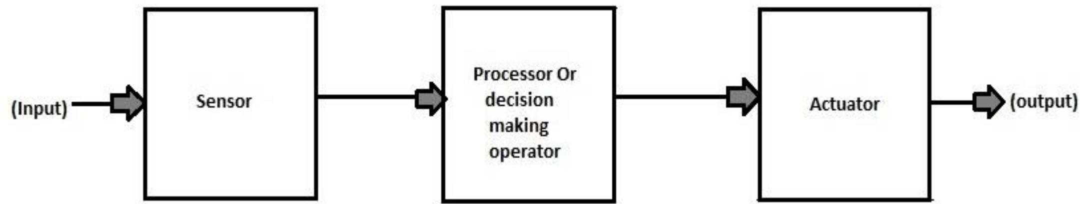

Fig. 1.1 Basic block Diagram of MEMS

1.2 INTRODUCTION TO CMUT (CAPACITIVE MICROMACHINED ULTRASONIC TRANSDUCER)

A CMUT is designed as an alternative to conventional piezoelectric transducers. Piezoelectric transducers have commercially been used for detecting and imaging of various objects such as water-trees in underground cables. However, they are known to have several drawbacks e.g. poor acoustic matching, dimensional limit. CMUT comparatively new concept of ultrasonic transducers. CMUTs can be regarded as the transducers in which the energy transformation takes place because of variation in capacitance. CMUTs are built on silicon substrate with help of micromachining technique. A cavity is created on silicon substrate, and a thin film suspended on its top act as a membrane on which a metalized layer functions as an electrode, along with the silicon substrate acting as a bottom electrode. Application of AC signal across the biased electrodes generates ultrasonic waves in the required medium. Thus, this will work as a transmitter. Whereas, application of ultrasonic waves on the membrane of biased CMUT will result in an alternating signal as the capacitance of the CMUT is changed thus acting as a receiver of ultrasonic waves.

Since CMUTs are micromachined devices, 2D and 3D arrays of transducers can easily be constructed with help of this technology. Huge numbers of CMUTs can be incorporated in a transducer array to provide wider bandwidth in comparison to former transducer technologies. Attaining a high frequency operation with CMUTs is simpler because of its smaller proportions. The operation frequency is dependent on the cell size (cavity of membrane), and on the rigidity of the material which is utilized as membrane. The incorporation of electronics is easier in case of CMUTs as compared to rest transducer technologies as these are built on silicon. The property of CMUTs to be used in high frequency accompanied by large bandwidth makes it an

excellent option as a transducer in field of medical imaging, particularly in the IVUS due to its wider bandwidth.

Ultrasonic transducer converts electrical energy into ultrasonic or acoustic energy and vice versa. These are available in a range of forms and sizes varying from single-element-transducers for mechanical scanning and linear arrays, to multidimensional arrays for electronic scanning. Though performance of an ultrasonic scanner is crucially dependent upon arrays/transducers, performance of arrays/transducers has been one of the bottlenecks which avert existing ultrasonic imagers from achieving the theoretical resolution limit. The principal reason for this is that design and fabrication process for medical ultrasonic array/transducer is of a broad interdisciplinary nature and need knowledge from a variety of fields, such as electrical engineering, acoustics and vibration, medical imaging, anatomy and physiology and material sciences and engineering. So far, the design of transducers is still mostly empirical and usually involving a trial and error approach.

1.3 IMPORTANCE OF CMUT

CMUTs are good alternative for chemical sensor applications due to their low motional impedance, exceptional mass sensitivity per membrane area, and high quality factor in contrast to rest flexural-mode resonators.

The main advantages of the CMUTs lay on the easiness to integrate them with CMOS, their manufacturability using microelectronic fabrication methods that allow repeatable results and a better performance, regarding bandwidth, frequency range and dynamic.

Thin plate is supported by a vacuum cavity where only the plate top is allowed to interact with the surrounding medium; thereby reducing the overall energy loss and resulting in a higher quality factor in comparison to cantilevers.

The device is composed of a large number of resonators parallel connected with each other. As a result of multi-resonator structure, a wide range of electrical impedance is available for matching to electronics and an enhanced reliability is achieved in comparison to a single resonator structure.

A repeatable and unfailing fabrication process guarantees a single resonant frequency along with a high quality factor for the lumped signal of the multi-resonator system.

1.4 APPLICATIONS OF CMUT

1. Ultrasonic phased array transducers are essential ingredients in modem medical diagnostic devices. For example, phased array sensors are used in ultra-solography for imaging of the fetus in a pregnant mother's womb.
2. CMUT can be used as chemical sensor [2].
3. Ultrasonic transducers are attractive for micro-scale applications since there CMUT can be used for determining viscosity, temperature and sound speed of the liquid [3].

1.5 GAPS IN STUDY OF CMUT

Capacitive sensors use large space of silicon wafer for bulk Micromachining, which requires large pieces of silicon to be etched. Hence making the total process expensive and unemployable for practical purposes.

These are electronically more complicated to design and fabricate. Effects of top electrode on membrane and effects of different sizes of electrode on membrane need attention which has not been dealt till date.

Optimization of physical parameters such as thickness of membrane, thickness of cavity, effect of area on top electrode is new research area which offers improvements over current standards.

Optimization of these parameters can lead to evolution of designs according to particular application.

1.6 THESIS SIGNIFICANCE

This thesis aims at resolving issues which put limitation in this technology application in practical scenario.

Thesis work starts with membrane shape drawn from important design parameters and frequency analysis. Results discussed in chapter 6 verifies graphically that correct resonance frequency is derived.

It lays attention on three geometries viz: Square, Circular and Hexagonal. Comparison of these three has been done to find the most optimum and appropriate geometry.

Chapter 6 establishes that Hexagonal is best and then three membrane materials viz: Silicon Nitride, Silicon and Polysilicon are compared over Hexagonal geometry for best material properties.

1.7 THESIS OUTLINE

This work is divided in total of seven chapters.

Chapter 2 is literature review, which gives details on the publications in this field. All the research work and papers which are being published in this area are listed chronologically in this chapter.

Chapter 3 discusses principle of operation of CMUT. Mathematical derivations are included to detail the CMUT process. Technical terms such as pull-in voltage, resonant frequencies etc. are introduced mathematically in this chapter.

Chapter 4 gives a description of the COMSOL multiphysics. Also it covers the research methodology used in this project. Finite element analysis (FEA) package of COMSOL Multiphysics is used for design and simulation of CMUT. Different modules and physics are also described in this chapter.

Chapter 5 describes the fabrication steps to design CMUT for immersion applications.
Chapter 6 presents the results and discussions of the simulation work.

Chapter 7 concludes this project after all results discussed in Chapter 6. Also it gives idea about future work possible in this field.

CHAPTER 2

LITERATURE SURVEY

This chapter lays emphasis on all the work that has been carried out in this area till date. It starts with the first paper published in 1994 till the one published recently. All the papers are presented chronologically in this chapter to include all the details and findings that has evolved in this area.

Capacitive transducers were first developed in the 1950's [4]. With the advent of MEMS technology, this sensor was miniaturized in the early 1990's [5]. Much of the work came from Khuri-Yakub's group at Stanford University.

In **1994**, **D.W. Schindel and D.A. Hutchinst** proposed non-contact inspection system for the characterization of thin solid material. This system utilised wideband air-coupled ultrasound, the generation and detection of which, were carried out on opposite sides of the sample (in the through-thickness mode) with help of Micromachined air-coupled capacitance transducers. With the resulting bandwidth, it was possible to estimate absolute velocities and thickness changes with an accuracy of 21% for wood products, polymers, glass, and CRP composites. It also resulted in a considerable increase in sensitivity for tone burst operation when the frequency matched the sample's through-thickness resonance. This system was used for the imaging of defects in composite materials [6].

In **1995, D.W. Schindel *et al.*** discussed both piezoelectric air-coupled devices and Micromachined air-coupled capacitance transducers for formation of images of artificial graphite foil defects in a fibre-reinforced thermoplastic composite plate. Tone burst excitation at the fundamental through thickness resonant frequency of the plate was used for this process. It was found that there are various advantages associated with the capacitance transducers in materials characterization. These advantages are a result of the wide bandwidth offered by them and consist of the capability to vary the excitation frequency for match with higher order resonant modes of the plate [7].

In **1999, X. Jin *et al.*** discussed numerous pioneering steps for fabrication of SMCUI transducers. Major steps required in device fabrication for optimization of transducer performance were investigated. These steps included electrode metallization, vacuum sealing and membrane formation. Three structures of transducer membrane were evaluated: a polysilicon membrane with an oxide SL, a nitride membrane with a polysilicon SL, a nitride membrane with an oxide SL. Three vacuum sealing mechanisms, each requiring a different level of lithographic sophistication and a different sealing mechanism were also investigated. These resulted in a sealed cavity to achieve a transducer dynamic range in excess of 100 dB around 4.5 MHz [8].

In **1999, O. Oralkhan *et al.*** experimentally characterised a 400 μm × 400 μm 2-D Capacitive CMUT array element and compared the results with theoretical predictions. The transducer exhibited a displacement sensitivity of $1.8 \times 10^{-7}\ \mathrm{nm}/\sqrt{\mathrm{Hz}}$ as a receiver and produced an output pressure of 16.4 kPa/V at the surface of transducer at 3 MHz, when acts as transmitter. This transducer also resulted in fractional BW of greater than 100% around 3 MHz, making it appropriate for use in ultrasound imaging [9].

In **2000, T. H. Gan *et al.*** proposed a technique for pulse-compression and applied it to air-coupled testing of solid materials. Wide BW swept-frequency signals (chirp) were generated in air with help of capacitance transducers to measure and image solid samples in through transmission. The proposed technique resulted in an improvement in SNR and timing accuracy for air-coupled testing. Images of defects for a variety of materials, including carbon-fiber composites and metals were obtained. Combining pulse-compression technique with capacitive transducers proved a powerful tool for non-contact air-coupled ultrasonic measurements [10].

In **2004, M. Wilm *et al.*** reported 3-D modelling of periodic arrays of CMUTs for operation in fluids. Modelling of bi-periodic transducer arrays was performed and radiation into any stratified media at the back-side as well as the front-side of the device was taken into account. The reported model was based on FEA/ BEM and was applied to MUTs based on silicon-nitride circular-membrane arrays on a silicon substrate operating in water. The spectrum characteristics of MUTs demonstrated

very-large-band emission, which was previously achieved by many authors. Guided modes were identified, that depended on the excitation conditions, which do not radiate in water. These modes were able to generate considerable cross-talk effects. The authors analysed the origin and nature of these guided modes to study the actual operation of MUTs [11].

In **2005, B. Bayram *et al.*** developed CMUT to meet high demands of Ultrasonic Industry. Bias voltage should be close to the collapse voltage to obtain maximum efficiency in CMUT. Authors extracted the pressure on CMUT surface taking care of attenuation and diffraction losses. Finally, authors found that collapse snapback operation of CMUT was better than conventional operation as it generated 1.04 MPa amount of pressure whereas it was only 0.47 MPa for conventional operation [12].

In **2005, A. S. Ergun *et al.*** introduced CMUT as the major candidate for upcoming generation imaging systems. The authors focused on two main fabrication processes for CMUT. These were water bonding method and sacrificial release process [13].

In **2005, I. Cicek *et al.*** presented integration of 2D CMUT arrays with front-end electronics. The design and verification of a front-end drive-out IC using 2D CMUT arrays was demonstrated for 3D ultrasonic imaging. The circuit cell of a single CMUT array element comprised of a low-noise readout amplifier and a high-voltage pulser. An electrical model of CMUT was developed with help of parameters derived through FEA, and both pre and post-layout verification were performed. An experimental chip was created for initial studies which consisted of the designed circuit cells arranged in a pattern of 4×4 array and each cell occupied an area of 200×200 μm^2. The chip was programmed for fabrication in 0.8 μm, 50 V CMOS technology. The designed system proved appropriate for combination with CMUT arrays through flip-chip bonding and the CMUT-on-CMOS process [14].

In **2005, A. Caronti *et al.*** summarized design, fabrication, characterization and modelling of 1D CMUT linear arrays for use in the area of ultrasound medical imaging. The intrinsic advantages of CMUTs: high frequency applications, enhanced BW and aptness for new imaging modalities, prove their candidature as new generation arrays for acoustic imaging. With the progress in microfabrication field,

silicon-based electrostatic transducers can be fabricated which are equally competent with piezoelectric transducers in terms of performance. The feasibility of CMUT technology for use in diagnostic echo graphic imaging was demonstrated, though the complete process from silicon die to final probe is still in its juvenile stage to be applied practically [15].

In **2008, J. Chen *et al.*** introduced CMUT array for invasive medical diagnosis. The authors used mere 40µm thick substrate to develop ultrasonic transducer instead of bulky substrates. Benefits over conventional designs were obtained such as reduced cross talk due to miniaturisation of substrate surface. Also due to its inherited advantages it can placed close to target issue to record precise readings [16].

In **2010, X. Cheng *et al.*** developed CMUT array for the purpose of photo acoustic imaging. Being a small device of 100 µm thickness and 2.8-5mm × 8-18 mm area, it can be placed near to organ to detect correct reading. Carrying the advantage of being placed close to organ it can take reading which is inaccessible to ordinary transducers [17].

In **2010, D. S. Lin *et al.*** developed ideal encapsulation coating for CMUT [18].

In **2011, Bu-Sang Cha *et al.*** focused on fabrication and characterization of CMUTs with a perforated membrane, in air. Two kinds of CMUTs had been fabricated having PR/AR of 10% and 20% and their mechanical and electrical characteristics were analysed. It was found that PR of membrane has a significant influence on mechanical restoring force and electrostatic force of the device due to variation in area of membrane and electrodes. This also affects the frequency response and sensitivity of the CMUT device. An improvement in electrostatic force and mechanical restoring force was reported with a decrease in AR and increase in DC bias voltage [19].

In **2011, A. O. Manzanare** and **F. M. de Espinosa** designed a transducer with help of Helmholtz resonator principles to report an improvement in performance of air-coupled capacitive CUMTs utilizing resonant cavities. The characteristics of transducer vested in the cavity dimensions and numerous acoustic ports, having the form of holes in the CMUT plate. The advantage of MUMPs process is its low cost

allowing the fabrication of economic prototypes. The effects of the acoustic ports and resonant cavities in CMUTs were studied using acoustical measurements and laser Doppler vibrometry. FEA was used for simulations to verify experimental measurements. The experiments showed that the output pressure and BW in air can be enhanced by tuning the resonance frequency of the plate with the frequency of the Helmholtz resonator. An additional resonance was visible in the output pressure spectrum due to presence of new resonant cavities in the transducer. Analysis of the BW was done by computing the mechanical Q factor of the tuned CMUT, estimated as 4.5 in contrast to 7.75 for the vacuum-sealed cavity MUMPs CMUT [20].

In 2013, A. Bhuyan *et al.* presented 3-D imaging system utilizing CMUT technology to address the challenges faced in building of real-time VUI systems which need circuitry for simultaneous generation of ultrasound beams to be transmitted and processing of received echo signals. Two different approaches were followed to demonstrate the integration of front-end electronics and transducer. The transducer consisted of an array of 5-MHz CMUT with an 8 mm aperture size. The aperture was formed of a 32×32 array of 1024 elements and element pitch of 250 m. An IC includes a transmit beamformer and receive circuitry for overall noise performance of the system. Interfacing of the assembly with an FPGA and a back-end system (including DAS and PC) was done. The function of FPGA was to supply the digital I/O signals for the IC and processing of received echo signals was carried on by the back-end system. Reconstruction of the echo data was done via a phased array imaging approach to obtain the volume image. Imaging experiments were performed with help of wire and spring targets, a ventricle model and a human prostrate. Capturing of real-time volumetric images was achieved at a rate of 5 volumes/s [21].

In **2013, D. K. Kim *et al.*** reported an indirectly clamped CMUT with a high electromechanical coupling factor. An indirectly clamped diaphragm included a circular bottom plate hanging from a ring-type middle plate below the inner end of an annular top plate. This design allowed the bottom plate to vibrate in a piston like manner. In this way, the average gap variation between electrodes could be made larger than the average diaphragm displacement. The deflection shape of the proposed diaphragm mainly depends on two geometric parameters: the relative radial position of the idle plate and the ratio of the top and bottom plate thickness. Parameter

simulation results showed that the optimal inner-to-outer radius ratio of the annular top plate ranges from 0.4 to 0.6 for a top and bottom plate thickness ratio of 0.5–1.5. Simulations of 8 × 8 CMUT arrays showed that the ratio of the gap variation to the diaphragm displacement and the coupling factor were 1.62 and 2.49 times, respectively, than that for a conventional CMUT array. Measurements of static displacements of fabricated indirectly clamped diaphragms showed that the circular bottom plate moved uniformly as expected. In addition, immersion test results showed that the output pressure of a fabricated indirectly clamped CMUT array is 1.72 times higher than that of a flat clamped CMUT array under the same conditions. In conclusion, high transmission and reception efficiencies for a CMUT could be achieved using the proposed indirectly clamped structure [22].

In **2013, K. K. Park and B. T. Khuri-Yakub** presented an airborne 3-D volumetric imaging system based on CMUTs. For this purpose, 89-kHz CMUTs was fabricated where a single CMUT was composed of a circular single-crystal silicon plate having a radius of 1 mm and a 20 μm thickness, which is activated by electrostatic force through a 20 μm vacuum gap. The transmit sensitivity at 300V DC bias is measured as 24.2 Pa/V and 14.6 Pa/V when excited by a continuous wave and a 30-cycle burst respectively and the receive sensitivity for a 30-cycle burst was measured as 16.6 mV/Pa (-35.6 dB re 1 V/Pa) at 300-V DC bias. A 2-D array of size 26×26 was realized through scanning of a co-located transmitter and receiver mechanically. The measurement of a 1.6λ size target at a space of 500 mm demonstrated a lateral resolution of 3.17° and also illustrated good agreement with the theoretical point spread function. To show the capability of the imaging system, 3-D imaging of two plates at a distance of 350 mm and 400 mm was created. Use of 2-D CMUT array for practical 3-D imaging purposes in air, like HMI was experimentally demonstrated [23].

In **2013, A. Bybi** described a procedure for minimizing crosstalk between the individual elements of a piezoelectric transducer array. FEA was used to develop a 2-D model and predicted voltages were applied to the array prototypes formed of PZT 27 ceramic. A feasibility study was carried out to test the symmetric and asymmetric LPAs at operating frequency of approximately 450 kHz. Low frequency was used for

easy fabrication of transducer arrays. This approach offered active cancellation of crosstalk in transducer arrays to generate continuous waves even when fabrication defects were present. It was possible to reduce the crosstalk by about 6-10 dB. A multichannel generator can be used in ultrasonic imaging systems, to provide electrical signals which included both phased signals for focalizing and deflection of the acoustic beam associated with the correction signals [24].

In **2013, B.G. Jeong *et al.*** proposed an indirectly clamped membrane structure to obtain a piston-like motion, for enhancement of moving efficiency and discussed its reliability and performance issues. The proposed CMUT comprised of three parts: an upper plate, a circular moving plate and a ring-shaped bridge layer. The structure was expected to produce the piston-like and more flexural motion when the upper plate is connected vertically to circular moving plate through a ring-shaped bridge layer. This structure exhibited 14.7% wider fractional BW and 1.7 times higher output pressure in comparison to standard basic structure. Toughness of the structure and resistance to stress generated from humidity and temperature, were tested in environmental conditions. Also, accelerated long-term operating test was performed to estimate durability and lifetime of the device [25].

In **2013, K. K. Park *et al.***, made comprehensive comparison between conventional and collapse mode CMUT at 10 MHz in 1-D array [26].

In **2014, L. L. P. Wong *et al.*** experimentally demonstrated row-column addressed arrays for ultrasonic NDT applications and analysed 32 by 32 CMUT array designed for application in medical imaging. The CMUT array had a centre frequency of 5.3 MHz and could perform C-scan on test objects with holes having diameters of 1.0 mm and 0.5 mm. The aperture size of array transducer had a size of 4.8 mm by 4.8 mm and was capable of scanning an area of 4.0 mm by 4.0 mm. For an N by N fully addressed 2-D array, N^2 pairs of interconnection and supporting electronic components such as amplifiers and pulsers are required. This count is reduced to N for a row–column addressed array of the same number of elements. Although, the resulting field of view is limited by the aperture size, row–column addressed arrays and the row–column addressing scheme can be used as substitutes to of 2-D arrays for NDT applications [27].

In **2014, A. Bybi** ***et al.*** reported a new and simple electrical method to cancel cross talk in the acoustical arrays. The benefits with the new scheme is that it is possible to obtain accurate correction electrical voltages, as it measures average electrical quantities like impedance and current in contrast to displacement in each point at the surface of the radiated element. Also, there is no need of a laser vibrometer, which is expensive in terms of time as well as not accurate for displacement measurements in water. Fabrication of an array of seven elements, made of a conventional piezo-ceramic material PZT-27 was done. This array was similar to those used in NDT applications and medical imaging. An electrical method based on electromechanical equivalent circuits for piezo-electric materials and motional current measurements is applied to it. The results demonstrated the capability of the system to reduce crosstalk. Also, the system was robust and easy to implement [28].

In **2015, M. L. Kuntzan** ***et al.*** fabricated, modelled and experimentally evaluated unconventional acoustic sensor. The sensor is comprised of two vacuum-sealed capacitively transduced pistons coupled with each other by a pivoting beam. Fabrication of surface-micromachined prototypes was presented, followed by finite element modeling and experimental confirmation of successful vacuum sealing. Dynamic frequency response measurements were obtained using broadband electrostatic actuation and confirmed a first fundamental rocking mode near 250 kHz. Successful reception of airborne ultrasound in air at 130 kHz was also demonstrated, and followed by a discussion of design paths toward improved SNR beyond that of the initial proto types presented [29].

CHAPTER 3

OPERATING PRINCIPLE OF CMUT

The basic building block of a CMUT is a capacitor cell consisting of a metalized membrane (top electrode) suspended above a heavily doped silicon substrate (bottom electrode) as shown in fig. 3.1 [30]. A single element in the array contains a large number of small capacitor cells connected in parallel as shown in fig. 3.2 [30]. A top view of four elements of a 1-D CMUT linear array is shown in fig 3.3 [30].

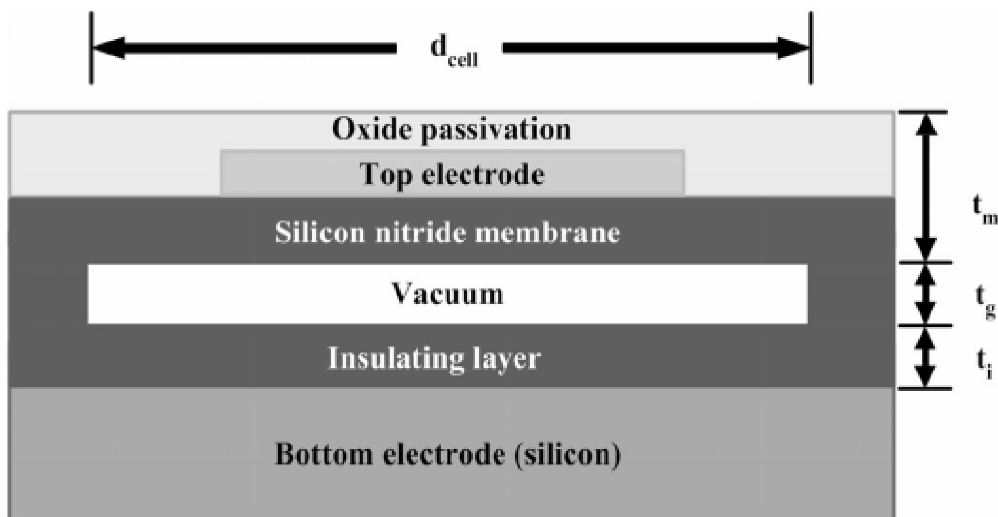

Fig. 3.1 Schematic cross section of a 1-D CMUT cell

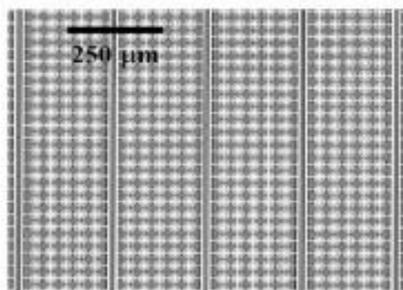

Fig. 3.2 CMUT cells connected in parallel

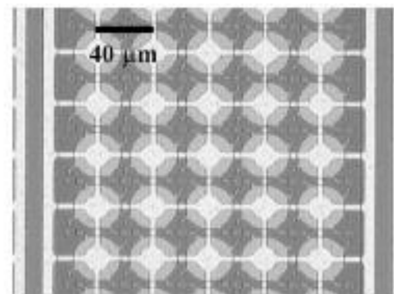

Fig. 3.3 Top view of CMUT cell

3.1 CMUT OPERATION

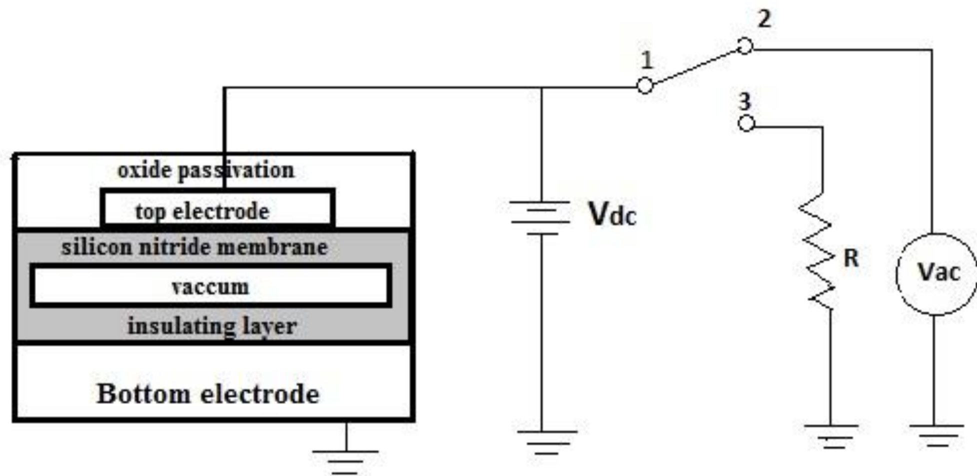

Fig. 3.4 Working principle of CMUT

Fig 3.4 [31] gives the brief description of working principle of CMUT. During CMUT operation, a direct current voltage is applied between the metalized membrane and the substrate. Due to electrostatic force, the membrane is attracted towards the bulk and stress induced within the membrane opposes this attraction. When the membrane is driven by an alternating voltage ultrasound is generated. If the biased membrane is subjected to ultrasound, it leads to generation of a current output because of the change in capacitance under a fixed DC bias voltage. The amplitude of this current output depends on the incident wave frequency, the capacitance of the device and the bias voltage [31]. ETR (Electromechanical Transformation Ratio) can be used to determine the efficiency of CMUTs. It can be expressed as the product of the capacitance of the device and the strength of electric field present across the gap beneath the membrane. It is possible to construct a thin membrane above a submicron sealed cavity through planar fabrication. This process is required for obtaining high electric fields in order to improve performance of transducer.

The CMUT can simultaneously be used for emission and reception of ultrasound. For emission, the membrane vibration is driven by an AC signal, and receive process is carried out by measurement of the deflection variation when pressure changes are induced on the membrane through the medium. A bias voltage is required by both the modes for proper working. Since, electrostatic attraction is uni-polar in nature, *i.e.*, forces are always attractive, a qualitative assessment would imply that, for unbiased CMUT, the membrane would vibrate at frequency double than the driving signal. This

is also shown through equations (3.1)-(3.9), by looking at the CMUT as a parallel plate capacitor where the suspended electrode can move without being deformed. Electric fringe fields can be ignored as an assumption for these equations. The value of the capacitance C between two plates is defined as:

$$C = \frac{Q}{V} \tag{3.1}$$

Where Q is the charge stored and V is the potential over the plates. The stored energy U by the capacitor can be expressed as:

$$U = \frac{1}{2}CV^2 \tag{3.2}$$

The electric field E is according to Gauss' law related to Q by:

$$E = \frac{Q}{\epsilon A} \tag{3.3}$$

where, ε is the permittivity of the medium between the electrodes and A is the area of the plate. It is also related to V:

$$V = Ed \tag{3.4}$$

where, d is the distance between the plates. Using the relations (3.3) and (3.4) in equation (3.1) we get:

$$C = \frac{Q}{Ed} = \frac{Q}{\frac{Q}{\epsilon A}d} \tag{3.5}$$

With the electrostatic force being unipolar, the magnitude of the force between the plates in the capacitor is equal to the absolute gradient of U with respect to the variable d. Using the relations (3.2) and (3.4) this results in:

$$F_{\text{electric}} = \left|\frac{\partial U}{\partial d}\right| = \frac{1}{2}\left|\frac{\partial C}{\partial d}\right|V^2 = \frac{1}{2}\frac{\epsilon A}{d^2}V^2 = \frac{1}{2}\epsilon A E^2 \tag{3.6}$$

The force is shown to be proportional to $E^2$and by taking into account that the electric field has two contributors, E_{AC} and E_{DC} an expression for E can be written:

$$E = E_{AC} + E_{DC} \tag{3.7}$$

$$E^2 = (E_{DC} + E_A\cos(wt))^2 \tag{3.8}$$

$$E^2 = E_{DC}^2 + E_A^2\cos^2(wt) + 2E_{DC}E_A\cos(wt) \tag{3.9}$$

If the DC component in (3.9) is set to zero, the vibration frequency becomes two times the frequency of driving signal. Thus, there is a need of biasing and for operation of device in linear regime, for its analysis without complete knowledge of its behaviour, E_{DC} must be greater than E_A [32]. When the CMUT is utilized as a receiver of acoustic waves, the variations in capacitance are measured to detect the vibrations in the membrane. In order to induce a current by the varying capacitance which can be read by the receiving circuitry, a constant bias voltage is required.

3.2 EQUIVALENT CIRCUIT OF CMUT

Single CMUT cell can be considered as lumped electromechanical model of ultrasonic transducer element as shown below in fig 3.5 [33].

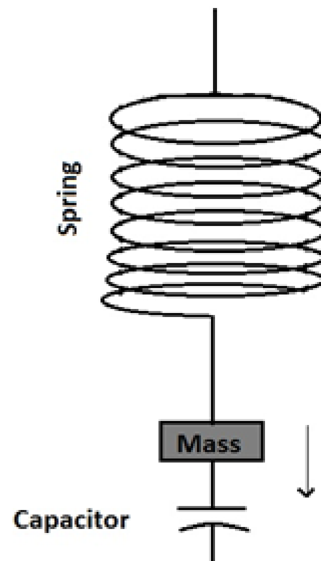

Fig. 3.5 First order lumped electromechanical model of transducer element

First order analysis emphasizes the major features of CMUT behaviour. It is assumed that the restoring force of membrane is a linearly dependant on its displacement and all electrical fringes fields and membrane curvature are neglected while considering the electrical force on the membranes. Further, all conductors and contacts are assumed to be perfect when MUT is supposedly operating in a vacuum, being similar as to neglect any loading of the membrane. Thus, the lumped electromechanical model is obtained which consists of a linear spring, a mass and a parallel plate capacitor. The mass is calculated by:

$$F_{capacitor} + F_{Spring} = F_{mass} \tag{3.10}$$

The stored energy is given by:

$$E = \frac{1}{2}CV^2 \tag{3.11}$$

where, C = capacitance and V = Voltage

According to virtual work, force applied by capacitor can be calculated by differentiation of potential of the capacitance w.r.t the position of mass.

$$F_{capcitor} = -\frac{d}{dx}(\frac{1}{2}CV^2) \tag{3.12}$$

Equation (3.12) can also be written as:

$$F_{capcitor} = -\frac{1}{2}SV^2\frac{d}{dx}\left(\frac{\varepsilon}{d-x}\right)$$

$$= -\frac{1V^2S\varepsilon(-1)}{2(d-x)^2}$$

$$= \frac{V^2S\varepsilon}{2(d-x)^2} \tag{3.13}$$

where, x= displacement, d=separation between the plates at rest, ε =permittivity and S= area of plates.

Also, $F_{spring} = -Kx$, where K is spring constant.

With help of equation (3.13), equation (3.10) can be written as:

$$\frac{V^2S\varepsilon}{2(d-x)^2} - Kx = m.a \tag{3.14a}$$

or, in terms of time

$$\frac{S\varepsilon[V(t)]^2}{2[d-x(t)]^2} - K[x\ (t)] = m.\frac{d^2x(t)}{dt^2} \tag{3.14b}$$

This is a nonlinear equation of second order. In order to obtain the significant quantitative behaviour of the system, following case is considered:

Put $V(t)=V_{DC}$ thus implying independence of time and leading to equation (3.15)

$$\frac{\varepsilon SV_{DC}^2}{2(d-x)^2}=K(x) \tag{3.15}$$

Equation (3.15) can be reorganized to give a polynomial of third degree in x, solution of which includes two regions of interest. If the value of V_{DC} is small, the solution gives three real roots, of these, only one is a feasible solution (the other roots

correspond to an unfeasible solution x>d and an unstable point). While value of V_{DC} is raised, a point comes at which the spring's restoring force is overcome by the electrostatic force leading to collapse of membrane. This point of inflection is established if a double real root is present such that x>d. The collapse point occurs when $X_{collapse} = d/3$. $X_{collapse}$ is the point beyond which electrostatic forces dominate the mechanical forces. For prevention of the capacitor from shorting just after collapse point occurs, we assume a thin insulating film of thickness t on one of the electrodes.

Softening effect occurs due to generation of a spring force in the −x direction as a result of the displacement of capacitor plate in the +x direction. Although, if V_{DC} is constant, this displacement causes a rise in the value of the electrostatic force in the +x direction. This increase in electrostatic force can be interpreted as a spring softening effect. A mathematical expression can be initiated by linearizing equation (3.14b) with help of Taylor expansion about the point x(t) = 0.

We know from Taylor theorem:

$$f(x) = f(a) + f'(x)f(x-a) \tag{3.16}$$

Therefore,

$$\frac{\varepsilon s V_{DC}^2}{2[d-x(t)]^2} = \left[\frac{\varepsilon s V_{DC}^2}{2d^2} + \frac{\varepsilon s V_{DC}^2}{2d^3}(x(t)-0)\right] \tag{3.17}$$

Using equation (3.17), equation (3.14) can be written as:

$$\frac{md^2x(t)}{dt^2} + \left[K - \frac{\varepsilon s V_{DC}^2}{d^3}\right]x(t) = \frac{\varepsilon s V_{DC}^2}{2d^2} \tag{3.18}$$

$$\left[K - \frac{\varepsilon s V_{DC}^2}{d^3}\right] = K_{soft} \tag{3.19}$$

Equation (3.18) becomes,

$$\frac{md^2x(t)}{dt^2} + K_{soft}x(t) = \frac{\varepsilon s V_{DC}^2}{2d^2} \tag{3.20}$$

Thus a reduction in system’s resonance frequency is expected as V_{DC} is raised. Such a shift in frequency is observed and reported in result section.

The membrane of thickness l_t is covered with a thin layer of conducting material on its top, and the distance between the bottom electrode and membrane is l_a. The value of capacitance is given by equation (3.21).

$$C(t) = \frac{\varepsilon_0 \varepsilon s}{\varepsilon_0 l_t + \varepsilon l_a} \tag{3.21}$$

where, ε is the dielectric constant of the membrane and S is the area of membrane.

Equation (3.22) gives the force of electrostatic attraction on membrane when V_{DC} is applied between the top and the bottom electrode.

$$F_E = -\frac{d}{dx}\left(\frac{1}{2} C V_{DC}^2\right) \tag{3.22}$$

After solving equation (3.22) we can write it as:

$$F_E = \frac{\varepsilon_0 \varepsilon s V_{DC}^2}{(\varepsilon_0 l_t + \varepsilon l_a)^2} \tag{3.23}$$

Let the voltage across the capacitor is V= (V_{DC} + V_{ac} sin ωt). Thus, the current flowing to the device can be given by

$$I = \frac{dQ}{dt} = \frac{d}{dt}\{C(t).V(t)\}$$

$$= C(t)\frac{d}{dt}V(t) + V(t)\frac{d}{dt}C(t) \tag{3.24}$$

for small signal analysis we can assume that

$$C(t)=C_0+C_{ac}\sin(\omega t + \varphi) \tag{3.25}$$

where, $C_{ac} <<< C_0$

Therefore equation (3.24) can be written as:

$$I = C_0 \frac{d}{dt} V_{ac}(t) + V_{DC}\frac{d}{dt} C_{ac}(t) \tag{3.26}$$

Differentiating equation (3.21), we get,

$$\frac{d}{dt} C_{ac}(t) = -\frac{\varepsilon_0 \varepsilon^2 s}{(\varepsilon_0 l_t + \varepsilon l_{a0})^2}\frac{d}{dx} l_a(t) \tag{3.27}$$

Here, l_{a0} is dc value of gap spacing. The derivative of air gap thickness is equal to membrane velocity.

$$\frac{d}{dt} l_a(t) = \bar{v} \tag{3.28}$$

$$I = C_0 \frac{d}{dt} V_{ac}(t) - \frac{V_{DC}\varepsilon_0\varepsilon^2 S}{(\varepsilon_0 l_t + \varepsilon l_{a0})^2} \bar{v} \tag{3.29}$$

Equation (3.29) is significant since it transforms velocity, a mechanical quantity into electrical current. Thus, we can define the transformation ratio as:

$$n = \frac{V_{DC}\varepsilon_0\varepsilon^2 S}{(\varepsilon_0 l_t + \varepsilon l_{a0})^2} \tag{3.30}$$

Number of turns can be controlled if the applied bias voltage is varied or the thickness of the membrane and air gap are changed. For completion of the equivalent circuit, it is required for the force and velocity at mechanical port to have some relationship between them. The equivalent circuit is shown in fig. 3.6 [34].

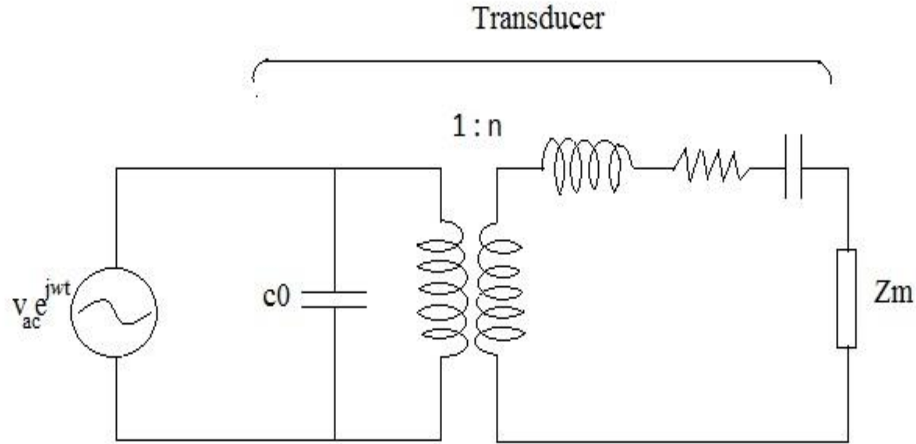

Fig.3.6 Equivalent circuit of CMUT

Under open circuit output conditions $Z_m \cong \infty$. The turns ratio related to transducer input to force per unit area on the medium is:

$\frac{F}{S} = P = nV$, where P=n/m^2, S= area, V = voltage and n= turns ratio

Mechanical impedance can be defined as the ratio between pressure and velocity. Mechanical impedance of the membrane is defined as [34]:

$$Z_m = \frac{P}{\bar{v}} \tag{3.31}$$

Amplitude of the pressure wave emitted from solid in to air gap is given by [34]:

$$P_{air} = \frac{2Z_{air}}{Z_m + Z_{air}} P_i \tag{3.32}$$

where, P_i is the amplitude of the incident wave, and Z_{air} is acoustic impedance of air.

3.3 IMPORTANT PARAMETERS OF CMUT

3.3.1 Pull-In Voltage

An important condition of parallel plate actuators or similar ones like the CMUT that should be kept in mind is pull-in. Pull-in occurs if the voltage over the device is increased to a point where the electrostatic forces pulling the electrodes together overcome the mechanical restoring force of the structure that suspends the moving electrode. This voltage is known as the collapse or pull-in voltage. When this condition occurs, the moving electrode or the membrane and the top electrode in the CMUTs case is pulled down to the bottom of the gap as shown in fig 3.7 [35]. It will stay there until the voltage is reduced to a lower level than the snap-back voltage of the device, as reported in [32].

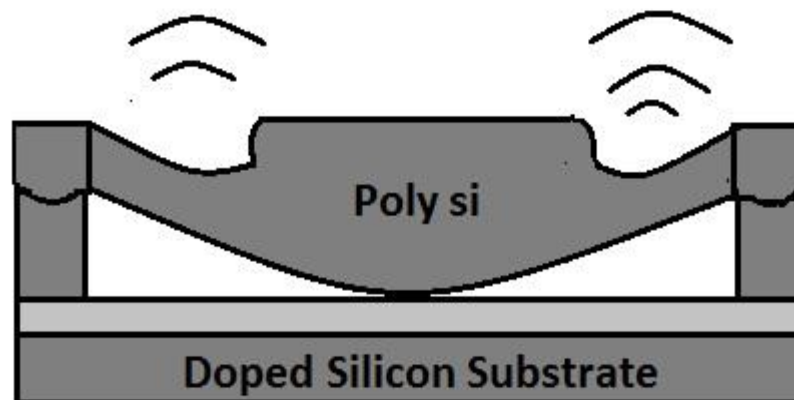

Fig.3.7 A cross-sectional view of collapsed mode CMUT

While in pull-in condition, the CMUT does not necessarily break down, but can continue to function as a vibrating ring, since the center of the membrane is pulled down to the bottom of the gap. Operation in this mode is reported in [36] to give a high coupling efficiency, and by that emits higher acoustic power compared to the traditional mode. However, for a CMUT designed to operate in the traditional mode, pull-in has to be avoided for the device to work.

For the membrane to be in equilibrium, the magnitude of the electrostatic force must be equal to the mechanical restoring force exerted by the inherent stress in the membrane. By assuming that the mechanical restoring force exerted by the inherent

stress in the membrane is linear, this force can be expressed as:

$$F_{mech} = -kx \tag{3.33}$$

Where k is the mechanical spring constant and x is the displacement. The electrostatic force (equation 3.6) can be rewritten as:

$$F_{electric} = \frac{CV^2}{2d} \tag{3.34}$$

We know that at equilibrium conditions:

$$F_{electric} = F_{mech} \tag{3.35}$$

Let d= $X + X_o$

From equation (3.33), (3.34) and (3.35), we have:

$$\frac{CV^2}{2(X+X_0)} = -k_m X \tag{3.36}$$

$$V^2 = \frac{-k_m 2X(X+X_0)}{C} \tag{3.37}$$

At a point, slope of F_{mech} =$F_{electric}$. The slope of $F_{electric}$ at this point can be defined as:

$$k_e = \frac{\partial F_{electric}}{\partial d} = \left|\frac{\epsilon AV^2}{2} . \frac{-2}{d^3}\right| = \left|\frac{\epsilon AV^2}{d^3}\right| = \frac{CV^2}{(X+X_o)^2} \tag{3.38}$$

The slope of F_{mech} at this point can be defined as:

$$k_m = \frac{\partial F_{mech}}{\partial X} \tag{3.39}$$

Using k_m and using equation (3.35) and (3.36), we can write:

$$k_e = C\left[\frac{-2k_m X(X+X_o)/C}{(X+X_o)^2}\right] = \frac{-2k_m X}{(X+X_o)} \tag{3.40}$$

$$k_e = k_m = \frac{-2k_m X}{(X+X_o)} \tag{3.41}$$

where,

$$X + X_o = -2X$$

$$X_o = -3X$$

This means plate is displaced by 1/3rd the total separation distanced when $V = V_{pull-in}$

Now from equation (3.40) we can write:

$$V^2 = \frac{-2k_m\left(\frac{-X_0}{3}\right)\left(X_0 - \frac{X_0}{3}\right)}{C} \tag{3.42}$$

$$V_{\text{pull-in}}^2 = \frac{4X_0^3 k_m}{9C} \tag{3.43}$$

$$V_{\text{pull-in}} = \frac{2X_o}{3}\sqrt{\frac{k_m}{C}} \tag{3.44}$$

Therefore, it is simpler to replace C, with $1.5C_o$, i.e., the original capacitance times 1.5, to represent capacitance value at $X_o/3$.

$$V_{\text{Pull-in}} = \sqrt{\frac{8k_m d_0^3}{27A\epsilon}} \tag{3.45}$$

3.3.2 Resonant Frequency

For a resonating structure like the CMUT, its behaviour depends on its structural dimensions and the medium it is operating in. In general, a resonant structure will have an increased resonant frequency with decreased dimensions, and the development of micromachining technology has made silicon structures resonating at ultrasonic frequencies possible. Equation (3.46) is a formula for resonant frequency of a circular membrane of uniform thickness t_m and shows the relation between the resonant frequency and membrane radius r [35].

$$f = \frac{0.47t_m}{a^2}\sqrt{\frac{E}{\rho(1-v^2)}} \tag{3.46}$$

where, a is the area, E is Young's modulus and v is the shear strain, ρ is density of the material. The system can be looked at as a spring system where the electrostatic attraction drives the system, the membrane acts as the spring, and the surrounding medium will cause dampening. If surrounded by a medium of low mechanical impedance like air for instance, the impedance of the membrane itself will dominate and a frequency response with a narrow peak around the center frequency is produce. If however the surrounding medium is a fluid, its impedance is much greater and will cause dampening of the system. This shifts the center frequency to a lower one and gives a broad banded frequency response around it. For the CMUT it is preferred to have a high center frequency since high frequency gives better resolution, and broad bandwidth means a high temporal resolution which makes detection of defects that are close together possible. One drawback with high frequencies is that ultrasound attenuation generally increases for increasing frequencies.

CHAPTER 4

DESCRIPTION OF COMSOL SOFTWARE

4.1 COMSOL MULTIPHYSICS

COMSOL is powerful tool which works on Finite Element Analysis (FEA), FEA is a method that can be used to obtain the solution to a large class of engineering problems involving stress analysis, heat transfer, electromagnetism and fluid flow .in pre-processing phase it create and discrete the solution domain into finite elements that is subdivided into nodes and elements, assumes a shape function to represent the behaviour of an element, develop equation for the element ,assume the elements to present the entire problem, apply boundary conditions, initial conditions and loading.in solution phase it develops a set of linear or nonlinear equations to obtain nodal results such as displacement values at different nodes. In post processing phase it obtains the other important information. COMSOL has packages (modules) for general physics applications which are based on advanced numerical method so it is known as "Multiphysics" [37]. The basic idea of this tool is to create virtual environment for the application under simulation.one or more physics can coupled easily in COMSOL. COMSOL also offer to add coupled system of PDE (partial differential equations).

Using desired physics interface, it is very easy to create models in COMSOL. According to the selected physics this tool has various equations although various expressions, variables and terminals can be defined manually in the tool. COMSOL basic window view is shown in fig. 4.1.

4.2 METHODLOGY OF WORKING ON COMSOL

First, user has to add his/her module with specific sub-physics (specific area of simulation or specific operation of that physics) and then user has to define study type for analysis. Some study options are listed below:

- Preset Studies
- Eigen Frequency
- Stationary
- Time Dependent

- Custom Studies
- Empty Study
- Eigen Value
- Frequency Domain

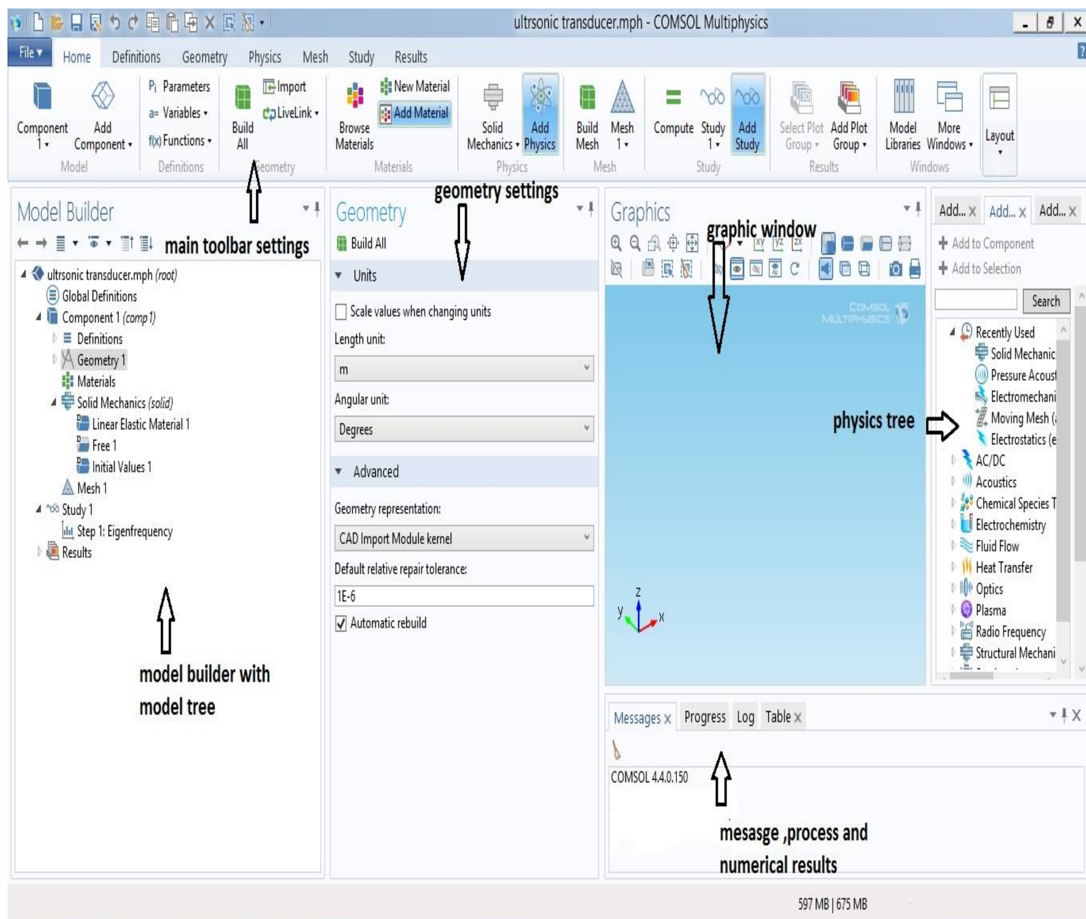

Fig. 4.1 COMSOL Multiphysics Window

One or more study can be selected and the result calculated in one study can be used in other study and one can change/add study during the simulation process. Each study has its default solver although user can modify the solver setting for particular problem and this is basically done in multiphysics simulations. One example of this is shown in fig. 4.2.

In the fig 4.2, study one is Eigen frequency analysis and solver is modified for solid mechanics calculation only and study 2 is prestressed Eigen frequency analysis and solver tree include the physics solid mechanics and electrostatics.

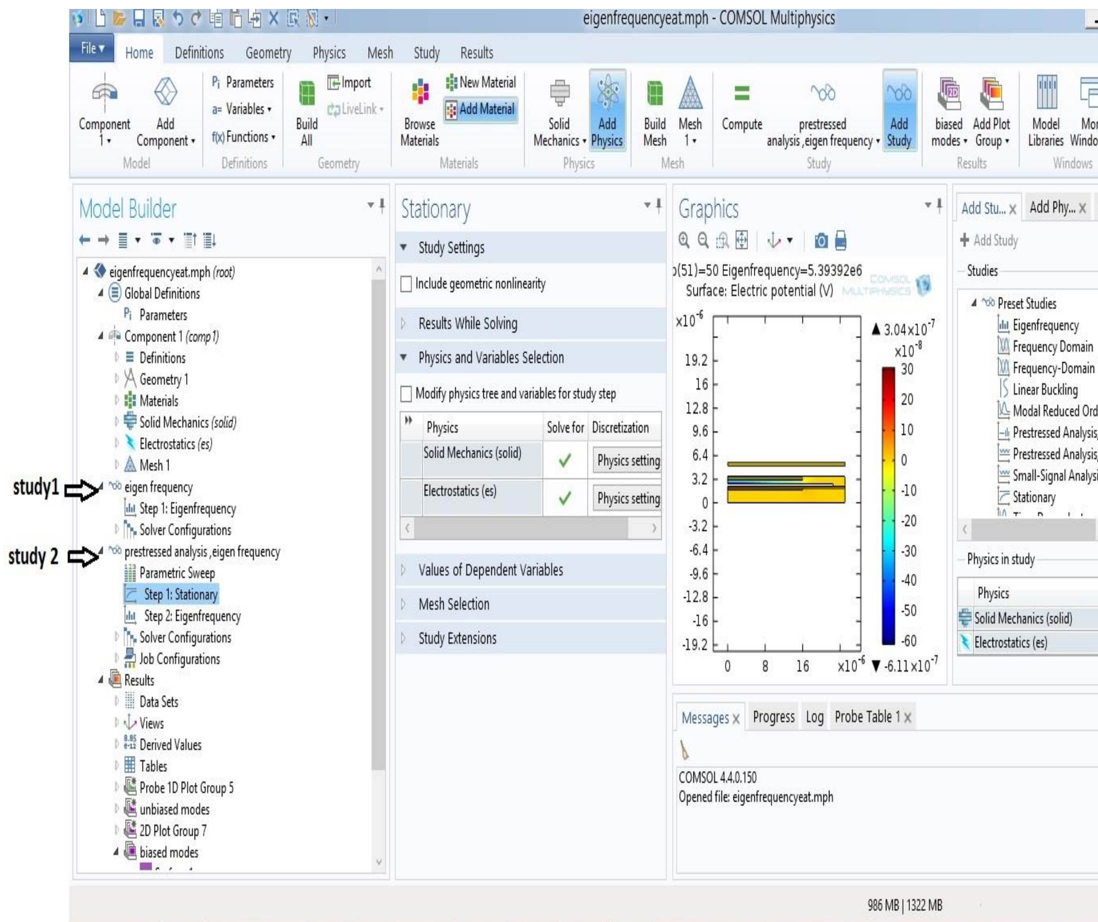

Fig. 4.2 Setup study type in COMSOL Multiphysics

4.3 BRIEF DESCRIPTION OF ALL MODULES IN COMSOL

- **Eigen frequency study:** It is used for computation of Eigen modes and Eigen frequencies of a linear or linearized model [37].

  Examples: In electromagnetics, the Eigen frequencies are related to the resonant frequencies and the Eigen modes are related to the normalized EM field at the Eigen frequencies. In solid mechanics, the Eigen frequencies are related to the natural frequencies of vibrations and the Eigen modes are related to the normalized deformed shapes at the Eigen frequencies.

- **Frequency domain study:** the Frequency Domain study is used to compute the response of a linear or linearized model subjected to harmonic excitation for one or several frequencies.

  Examples: In solid mechanics, it is used to compute the frequency response of a mechanical structure with respect to particular load distributions and frequencies. For quasi-static formulations in electromagnetics, it is used, for example, to

compute the impedance versus frequency. For acoustics and electromagnetic wave propagation, it is used to compute the transmission and reflection versus frequency. A Frequency Domain study accounts for the effects of all Eigen modes that are properly resolved by the mesh and how they couple with the applied loads or excitations. The output of a Frequency Domain study is typically displayed as a transfer function, for example, magnitude or phase of deformation, sound pressure, impedance, or scattering parameters versus frequency.

- **Prestressed Analysis:** Prestressed Eigen frequency study is used to compute Eigen frequencies and Eigen modes that are influenced by a prior static load. The study consists of two study steps: a stationary study step which is then followed by an Eigen frequency study step. This study computes the Eigen frequencies and the shapes of the Eigen modes when influenced by a prior static load on the structure.
- **Stationary study:** This study is used when there is no alteration of field variables with time. Examples: In electromagnetics, it is used for computation of static magnetic or electric fields, and direct currents. In solid mechanics, it is used for computation of stresses, strains and deformations, at static equilibrium. In heat transfer, it is used for computation of the temperature field at thermal equilibrium. In chemical species transport, it is used for computation of steady-state chemical composition in steady flows. In fluid flow, it is used for computation of the pressure fields and steady flow. In chemical reactions, it is used for computation of the chemical composition of a reacting system at equilibrium. It is also feasible to compute a number of solutions, like several load cases, or for tracking the nonlinear response to a slowly varying load.
- **Time Dependent study:** This study is used when there is alteration of field variables with time. Examples: In electromagnetics, it is used for computation of transient EM fields, including EM wave propagation in the time domain. In solid mechanics, it is used for computation of the time-varying deformation and motion of solids which are subjected to temporary loads. In heat transfer, it is used for computation of temperature variations over time. In acoustics, it is used for computation of the time-varying propagation of pressure waves. In fluid flow, it is used for computation of unsteady flow and pressure fields. In chemical reactions, it is used for computation of the chemical composition of a reacting system and

reaction kinetics. In chemical species transport, it is used for computation of chemical composition over time.

- **Eigenvalue:** The Eigenvalue study is used for computation of the eigenvalues and Eigen modes of a linear or linearized model in a generic eigenvalue formulation where the eigenvalues are not necessarily frequencies. The Eigenvalue study gives you full control of the eigenvalue formulation, in contrast to the Eigen frequency study that is adapted for specific physics interfaces. The Eigenvalue study is typically used for equation-based modeling.

COMSOL consists of list of modules that can be used according to the specific application list of these modules are listed below:

- AC/DC Module
- Acoustics Module
- Batteries & Fuel Cells Module
- CAD Import Module
- CFD Module
- Chemical Reaction Engineering Module
- Corrosion Module
- ECAD Import Module
- Electrochemistry Module
- Electrodeposition Module
- Fatigue Module
- Geomechanics Module
- Heat Transfer Module
- LiveLink Products for CAD
- LiveLink for MATLAB
- LiveLink for Excel
- Material Library
- MEMS Module
- Mathematics module
- Mixer Module
- Microfluidics Module
- Molecular Flow Module

- Multibody Dynamics Module
- Nonlinear Structural Materials Module
- Optimization Module
- Particle Tracing Module
- Pipe Flow Module
- Plasma Module
- RF Module
- Semiconductor Module
- Structural Mechanics Module
- Subsurface Flow Module
- Wave Optics Module

Capacitive Micromachined Ultrasonic Transducers are designed with the help of following modules mainly:

- AC/DC Module
- Structural Mechanics Module
- Mathematics Module

➢ **AC/DC Module:** The AC/DC interfaces are used to compute the electric and magnetic fields in static and low-frequency systems; that is, in systems where the wavelength is substantially larger than the studied device., the AC/DC interfaces can be used for modeling electrical circuits, electric current conduction, magnetic and electric fields with full vector formulations, orbits of charged particles, and rotating machinery such as motors and generators. Electrostatic physics is defined under this module.

➢ **Structural Mechanics Module:** This branch consists of physics interfaces for analyzing deformations, stresses, and strains of solid structures. Available analysis types include Stationary, Eigen frequency, Transient, Frequency response, and Linear Buckling. Solid mechanics is defined under this module.

➢ **Mathematics module:** The Mathematics branch contains interfaces for solving PDEs and ODEs, performing sensitivity analysis, modeling moving meshes and deformed geometries, and more. Moving mesh is defined in this module.

- **Electrostatics:** It is used for computation of the electric field, the electric displacement field and potential distributions in dielectrics under conditions where the electric charge distribution is clearly defined. The formulation is stationary but for use together with other physics, also Eigen frequency, frequency-domain, small-signal analysis and time-domain modeling are supported in all space dimensions. The physics interface solves Gauss' Law for the electric field using the scalar electric potential as the dependent variable.

Electrostatic equations

The electric potential, V, can be defined by following equation (under static conditions),

$$E = -\nabla V \tag{4.1}$$

When equation (4.1) is combined with the relation, $D = \varepsilon_0 E + P$, between the electric field E and electric displacement D, Gauss' law can be represented as the following equation:

$$-\nabla.(\varepsilon_0 \nabla V - P) = \rho \tag{4.2}$$

In equation (4.2), ε_0 denotes the permittivity of vacuum (SI unit: F/m), P denotes the electric polarization vector (SI unit: C/m^2), and ρ denotes space charge density (SI unit: C/m^3). Equation (4.2) illustrates the electrostatic field in dielectric materials. For in-plane 2D modeling, it is assumed that the electrostatics interface has an evenness such that the electric potential changes only in the directions, x and y and remains constant in the direction z. This means that E is tangential to the xy-plane. If this symmetry exists, the equation can be solved similarly to the 3D case. The equation (4.3) is solved by the interface where d is the thickness in the z direction.

$$-\nabla.\mathrm{d}(\varepsilon_0 \nabla V - P) = \rho \tag{4.3}$$

The situation is considered when the geometry and the fields are axially symmetric by axisymmetric version of the interface. For that case, the electric potential is invariable in the z direction, leading to the electric field being tangential to the xy-plane.

- **Solid mechanics:** The Solid Mechanics interface is aimed for general structural analysis of 2D, 3D, or axisymmetric bodies. In 2D, plane strain or plane stress assumptions may be utilized. The basis of Solid Mechanics interface lies in

solution of Navier's equations, and results such as stresses, strains and displacements are calculated. The MEMS Module, Structural Mechanics Module and Acoustics Module add several features, for example geometric nonlinearity and advanced boundary conditions such as contact, follower loads, and non-reflecting boundaries. With the Nonlinear Structural Materials Module or the Geomechanics Module, the interface is extended with, for example, material models for plasticity, hyperelasticity, creep, and concrete [37].

- **Moving mesh:** The Moving Mesh interface can be used to create models where the geometry, here represented by the mesh, experiences a change in shape because of some physics in the model. It may be used to study both kinds of deformations: and time-dependent and stationary states; where the change in shape of the geometry is caused by the dynamics of the problem.

4.4 COUPLING OF PHYSICS

As CMUT is an electromechanical system, therefore we couple the physics of electrostatics and solid mechanics to describe its dynamics as shown in fig.4.3.

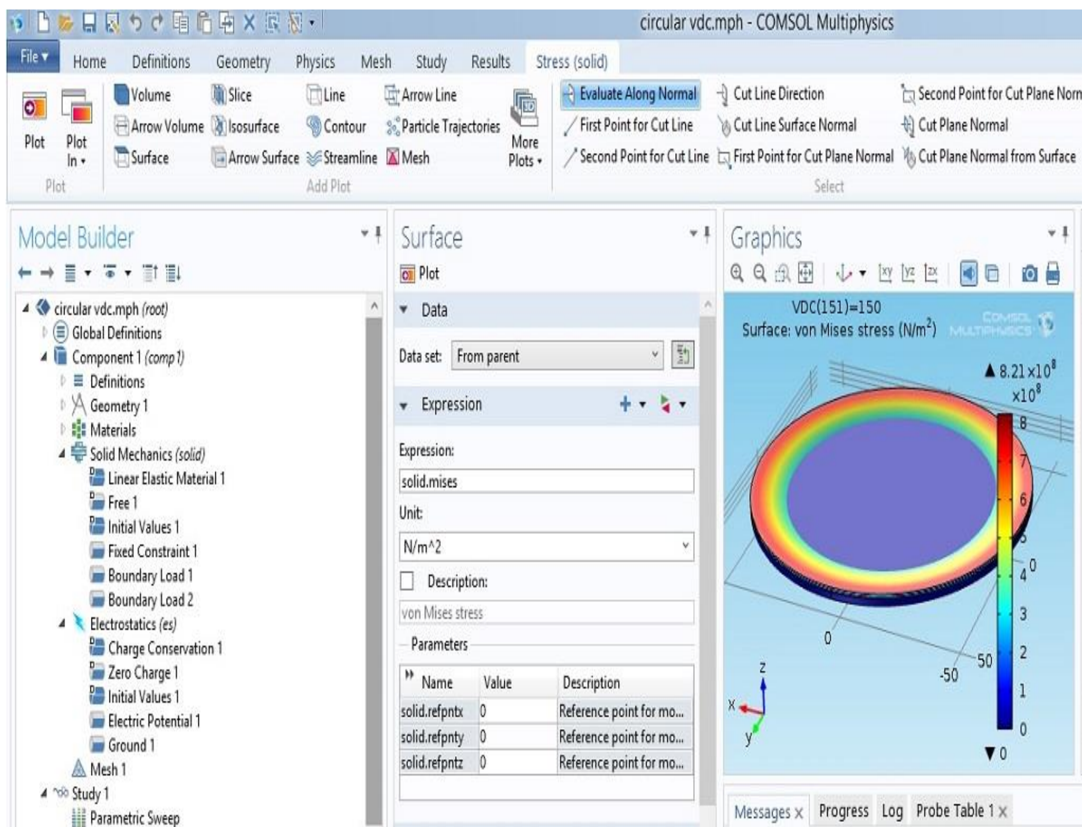

Fig. 4.3 Coupling of physics in COMSOL

- **Solid mechanics interface**
  - **Linear Elastic Material:** It denotes the default material, which includes a linear elastic equation for the displacements and consists of a settings window to describe the elastic material properties.
  - **Free:** This feature denotes the default boundary condition. Thus, it means that no loads and no constraints are acting on the boundary.
  - **Initial values:** This node is used for adding preliminary values for the velocity field and the displacement field which can function as a primary condition for a transient simulation or as a presumption for a nonlinear analysis initially.
  - **Fixed constraint:** This node is used for adding a condition that causes the geometric unit as permanent (fully constrained); i.e., for all directions, the displacements can be said as zero. This feature is used to fix the sides of the membrane and the bottom electrode.
  - **Boundary load:** This feature is used to add a boundary load to specific boundaries. The electrostatic forces calculated by "Electrostatic" physics are defined in this feature.

- **Electrostatic interface**
  - **Charge conservation:** This is the key feature, which allows addition of the equation for the electric potential and consists of a settings window which defines the constitutive relation for the electric displacement field and properties associated with it, like relative permittivity.
  - **Zero charge:** This node used for adding the condition when no charge is present on the boundary or, $n.D = 0$. When symmetry in potential is present, with respect to the boundary; then for symmetry boundaries, this boundary condition is applicable. At exterior boundaries, this denotes the default boundary condition. At interior boundaries, it denotes that displacement field cannot enter the boundary and that the electric potential is discontinuous across the boundary.
  - **Electric potential:** This node supplies an electric potential V_0 as the boundary condition $V=V_0$. Since, in the interface, solution of problem is being found out to compute the value of electric potential, its value is usually defined at particular portion of the geometry. For some particular interfaces, also select

further **Electric Potential** features can be selected from the **Edges** (in case of 3D models) or **Points** (in case of 2D models) submenus.

- **Ground:** It indicates that potential is nil on the boundary. It is also valid at symmetric boundaries where it is known that the potential is antisymmetric with respect to the boundary.

Conclusion: In this chapter, we have studied and discussed about the COMSOL multiphysics simulation tool with its features and different modules. As we will design and simulate different Capacitive Micromachined Ultrasonic Transducer geometries, this module will be helpful for analysing results and understand the behaviour of CMUT with respect to its properties.

CHAPTER 5

FABRICATION STEPS OF CMUT

Two main processes are used for the fabrication of CMUT *i.e.*, sacrificial surface micromachining and direct wafer bonding process. The wafer bonding process is mostly used for CMUT fabrication because it is well suited for HIFU (High Intensity Focused Ultrasound) which is desirable in medical applications. Wafer bonding process also enables different membrane shapes and topologies to be fabricated which increase the output pressure and increases the reliability of the device. Also the complexity is less in wafer bonding process since only 8 lithography masks are used as compared to the sacrificial process which requires 12 lithography masks [38].

The sacrificial release process has been the traditional method for fabricating CMUTs since the early 1990's. There are numerous versions of processes, all are based on same method. The cavity underneath the membrane is created by depositing or growing a sacrificial layer, membrane and substrate materials can be used to fabricate the CMUTs. Selection of these different materials and etchants influences the design process control and overall device yield. Typically silicon nitride membrane is used with polysilicon as the SL. Wet etch of Potassium Hydroxide (KOH) is used to release the membrane through a series of etch holes. These holes are then sealed using a silicon nitride deposition before the membrane is etched back to its final thickness.

The original CMUT process utilizes LPCVD process for sealing and membrane formation [8]. Since the high process temperatures (900°C) causes post process CMOS integration unfeasible, also major disadvantage to this scheme is that fabrication process is very complicated. A newly developed method based on PECVD silicon nitride produces a comparatively huge gap of 4000 Å.

A new approach to fabrication of CMUT utilizes the technique of wafer-bonding in order to enhance uniformity of membrane [39]. Although, post process CMOS integration is not feasible due to the high temperatures needed for bonding. One more way for electronics integration is fabrication of the CMUT out of the layers of a standard CMOS process [40]. Though, this comprises of the ultimate in electronics integration, it is not possible to fabricate the CMUTs directly over the electronics, as it leads to waste of expensive real estate on the chip. Another approach to electronics

integration is post processing of CMUTs directly over CMOS electronics [41]. Here, polymer SLs are used under a silicon nitride membrane which is built with help of PECVD process, but due to gap generation in the range of 1–2μm, it is not appropriate for efficient operation of CMUT at higher frequencies. For high frequency operation of CMUT, small and stiff membranes are required to reach the desired resonant frequency. Prohibitively high-collapse voltages are required by these membranes, which are coupled with large gaps, for efficient operation of CMUT. The process of fabrication of CMUT is explained below and illustrated with help of fig. 5.1 [42].

5.1 FABRICATION PROCESS FLOW

Step 1: Formation of Bottom Electrode

The very first thing in the process of fabrication is formation of the bottom electrode. It can be formed either by patterning a thin layer of metal or by doping the silicon substrate. If it is a doped silicon electrode, all unmovable elements of the top electrode function as parasitic capacitance which causes degradation in performance of device. To lessen the mentioned hitches, a patterned, metal-bottom electrode is utilized. Through patterning, a significant reduction in the parasitic capacitance is possible.

Step 2: Insulating Layer

Deposition of a 1500 Å thick silicon nitride layer is carried for protection of the silicon substrate or bottom electrode from the etchants utilized during the process of membrane release. If a doped Si bottom electrode is utilized in combination with an amorphous Si-SL, there is a need of silicon nitride layer for prevention of the etching of the silicon substrate from TMAH (Tetra-Methyl Ammonium Hydroxide).

Step 3: Sacrificial Layer

The sacrificial layer (SL) is used for creation of the gap under the membrane and can be built with either sputtered metal or PECVD amorphous silicon. Amorphous Si can be deposited at low temperatures (300°C) but needed to be patterned with a RIE. The surface roughness of PECVD amorphous Si is low (approximately 4Å) and when coated with silicon nitride, its oxidation is prohibited. It is possible to form gaps as

small as 1000Å with help of this film. The only drawback of using amorphous Si is that TMAH is poorly selective during the membrane release.

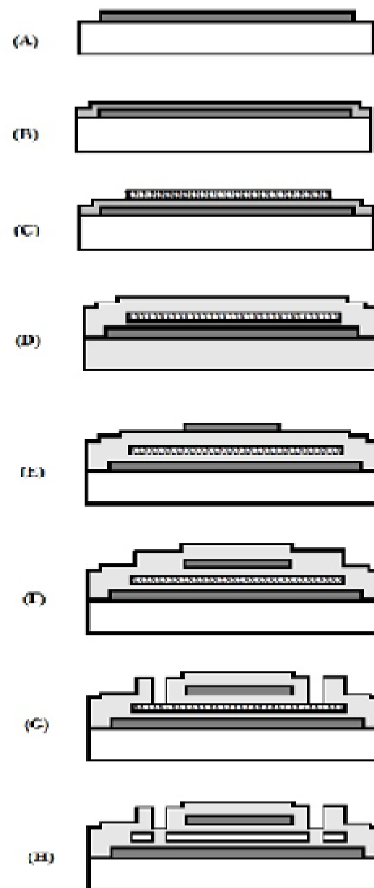

Fig. 5.1 Low temperature process flow illustration for immersion CMUT.

As discussed previously, Al is a not a good alternative for a SL because when it is coated with silicon nitride, rigorous oxidation occurs. Some researchers have effectively employed Al as a SL [43]. Although, for such applications, large gap height (~1µm) is required, and surface oxidation is not of more importance. There is no oxidation of Cr in the PECVD chamber and hence, it can easily be patterned with help of wet etchants available commercially. The Cr etchant shows selectivity to silicon nitride and, thus, is an appropriate release agent. Small gaps (~1300 Å) can be fabricated with help of Cr-SL, although this is not the lower limit. Generally, the static deflection of the membrane limits the gap height, due to residual stresses, the surface roughness of the SL, stiction and atmospheric pressure. Residual stresses causes the static deflection which can be eliminated by proper designing; and the problem of stiction can be eliminated by first release of a thicker membrane, and then thinning it back to the requisite thickness after sealing. Roughness of the surface of the SL is of the order of nm and signifies maximum gap height.

Step 4: Membrane Formation

If PECVD silicon nitride is deposited over the SL, CMUT's vibrating membrane is formed. The thickness of the layer can vary, according to the application, but it has a typical value of 6000Å. For prevention of defects in silicon nitride layer, it is needed that any photoresist residue is completely removed before the deposition. When amorphous Si is utilized as the SL, a Piranha clean or standard RCA can be used for this process. Though, if a metal SL is used, these cannot be used as they cause degradation or removal of the metal layer. Hence, the residue of photoresist is get rid of by submerging the wafers in acetone beaker in an ultrasonic bath. Photoresist strippers which are available commercially can also be utilized. The wafer is taken out after soaking for few minutes and cleaned with methanol, deionized water and acetone. The layer of silicon nitride can be placed over SL, after the wafer is dried.

Step 5: Formation of Top Electrode

Here also, Al is a not a good alternative as the material for top electrode as its oxidation will occur with successive silicon nitride depositions. Cr also is not suitable as its residual stress and resistivity are high. Though, the conjunction of these two can provide an appropriate top electrode. Deposition of 1200Å of Al followed by 300Å of Cr builds the top electrode. The Al offers the advantage of good electrical conductivity, and its oxidation is prevented by Cr layer.

Step 6: Second Membrane Deposition

One more layer of silicon nitride is deposited for increase in the thickness of the membrane and protection of the top electrode from the etchants used during release. The typical thickness of silicon nitride layer is 6000Å.

Step 7: Membrane Release

To enable the etchants to get to the SL, etching of holes through the layers of silicon nitride is done with help of RIE. If an amorphous Si-SL is utilized, the selectivity of the etch process to Si should be known. If it has low selectivity, etching can be easily done through the thin layer of SL, isolating silicon nitride, and downwards to the Si substrate. When it happens, the silicon etchant (release agent) will interact with the

substrate and leads to destruction of the devices. If a metal SL is used, the selectivity of the RIE is of less concern since the metal layer functions as an etch stop.

Step 8: Membrane Sealing

The membranes need to be sealed for applications in immersion technology; by deposition of one more film of PECVD silicon nitride. The thickness of sealing layer is typically more as compared to the gap height (4500Å vs. 1500Å) and guarantee absolute sealing of membrane with a single deposition. The CMUTs are generally sealed with help of LPCVD silicon nitride depositions, though in that case, long etch channels are required for prevention of deposits underneath the membrane. Use of materials like LPCVD silicon dioxide cause better localized sealing as compared to that provided by silicon nitride, although the requirement of higher temperatures forbids the post CMOS electronics integration. The end action in the process utilizes RIE for etching through the silicon nitride layer which covers the bond pads. It permits making of external electrical connections with wire bonding. For particular cases, gold was used for patterning over the bond pads for improvement in the trustworthiness of the wire bonds.

CHAPTER 6

RESULTS AND DISCUSSIONS

6.1 SHAPE AND MATERIAL OF MEMBRANE

6.1.1 Shape of Membrane

Shape of membrane is important design parameter for CMUT and it can be square, circular and hexagonal and we will discuss the effect of these three shapes on resonance frequency. The area utilization of three shapes is listed below:

Table 6.1 Area utilization of various shapes

Geometry	**Area**	**Percentage of circular area**
Circular	$3.14r^2$	100
Square	$2r^2$	63.7
Hexagonal	$2.6r^2$	82.8

6.1.2 Membrane Materials

Silicon, silicon nitride and polysilicon are the materials that are used for membrane.

Silicon is perfect hookean material that when it is flexed, there is virtually no hysteresis and hence, no energy dissipation. As we discussed already, CMUT is an electromechanical system, and because of highly repeatable motion of silicon makes it attractive in MEMS application. The basic techniques for providing all silicon based MEMS devices are deposition of material layers patterning of these layers by photolithography and then etching to produce required shapes.

- Silicon is mechanically stable material.
- Ideal structure material, light as aluminium
- Silicon shows virtually no mechanical hysteresis. It is thus an ideal candidate material for sensors and actuators.

Silicon nitride: This material is electrical insulator and is does not wet by nonferrous alloys silicon nitride is a rather expensive material but its performance to cost benefit ratio is excellent in the applications, where it can perform the normally utilized material with long life and very reliable low maintenance operation.

- High hardness
- High fracture toughness
- Good chemical resistance
- High strength over a wide temperature range.

Polysilicon: Polysilicon is an aggregation of pure silicon crystals with randomly orientations deposited on the top of silicon substrate. It is basically highly doped silicon. Being randomly oriented, polysilicon is even stronger than single crystals.
The mechanical properties of this material are listed below:

Table 6.2 Mechanical properties of different materials

Materials	**Young's modulus (GPa)**	**Poisson's ratio**	**Density(kg/m^3)**
Silicon	129.5 <100> 168.0 <110> 186.5 <111>	0.3	2330
Silicon nitride	304-310	0.27	3300
Poly silicon	160-165	0.25	2320

6.2 FREUQNCY ANALYSIS OF MEMBRANE DESIGNS AND SIMULATIONS RESULTS

For a resonating structure like the CMUT, its behaviour depends on its structural dimensions and the medium it is operating in. In general, a resonant structure will have an increased resonant frequency with decreased dimensions, and the development of micromachining technology has made silicon structures resonating at ultrasonic frequencies possible. Recalling equation (3.46) we can write:

$$f = \frac{0.47t_m}{a^2}\sqrt{\frac{E}{\rho(1-v^2)}} \quad (6.1)$$

The equation (6.1) is for circular membrane and here, E is Young's modulus and a is the radius of the membrane and v is the poisson's ratio and ρ is density of the material.

6.2.1 Simulation Results for Three Membranes

1) Circular Geometry

This Simulation is carried in COMSOL for circular shape of membrane with all parameters set as the following:

Frequency: 1.31418e6 Hertz

Radius: 56.4µm

Thickness: 1µm

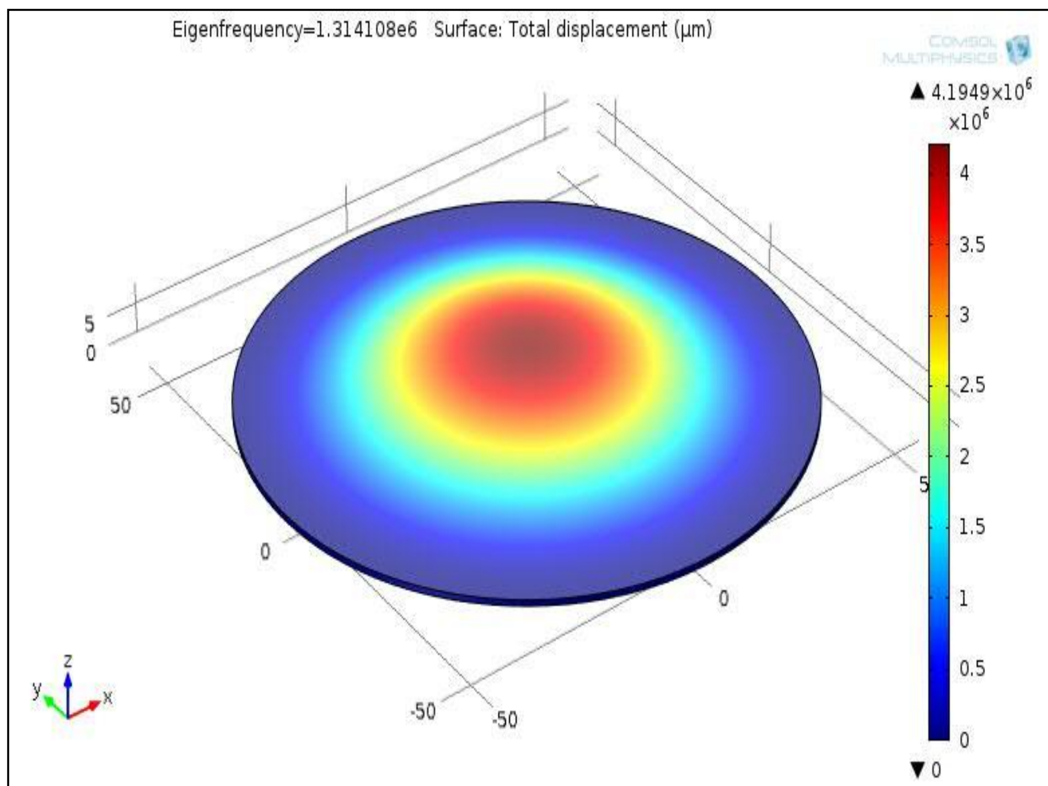

Fig. 6.1 Simulated circular membrane

2) Square Geometry

This Simulation is carried in COMSOL for square shape of membrane with all parameters set as the following:

Frequency: 1.47245e6 Hertz

Side Length: 100µm

Thickness: 1µm

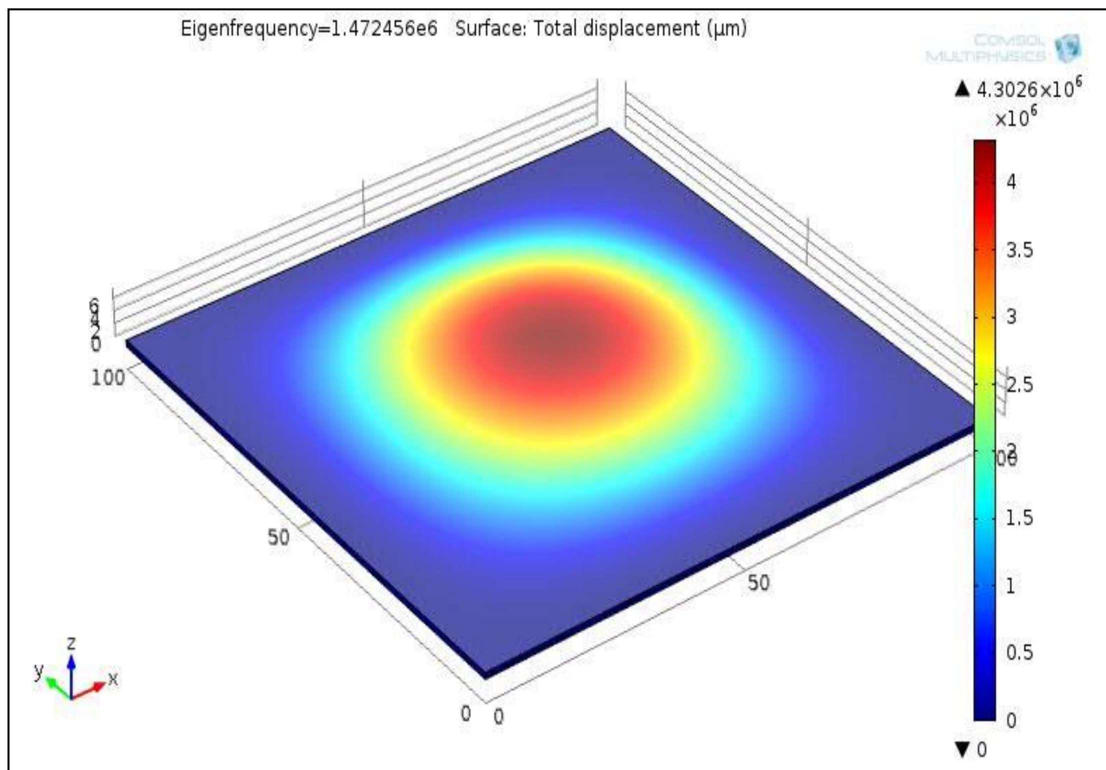

Fig. 6.2 Simulated square membrane

3) Hexagonal Geometry

This Simulation is carried in COMSOL for hexagonal shape of membrane with all parameters set as the following:

Frequency: 1.363994e6 Hertz

Side Length: 62µm

Thickness: 1µm

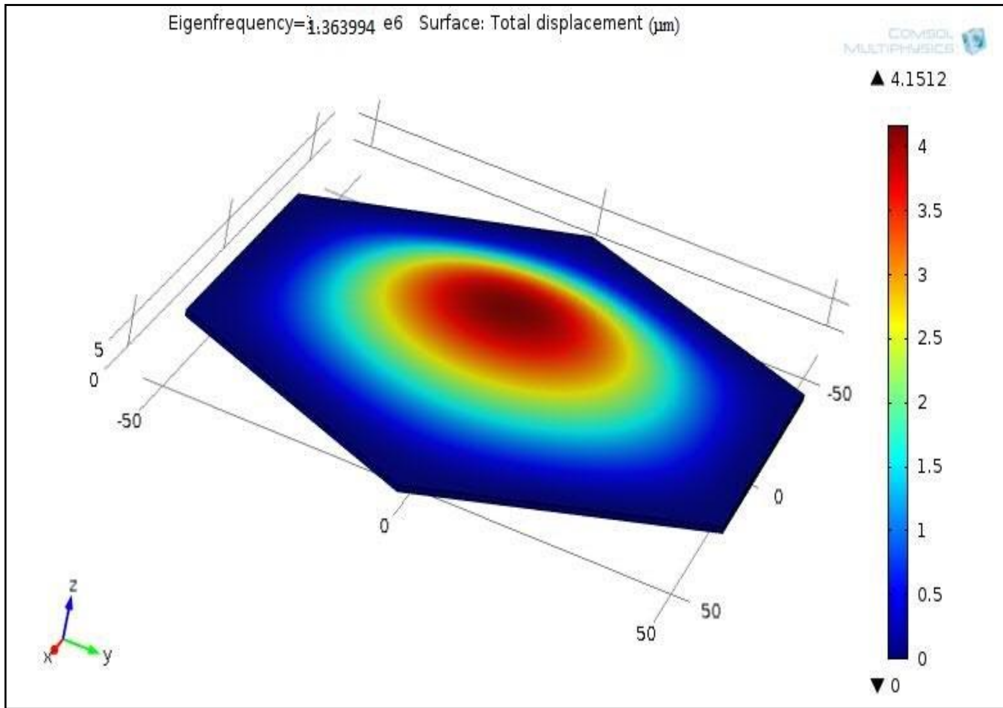

Fig. 6.3 Simulated hexagonal membrane

6.2.2 Frequency Analysis of Different Membranes

The graph of frequency versus deflection for the above discussed membranes is given in fig. 6.4.

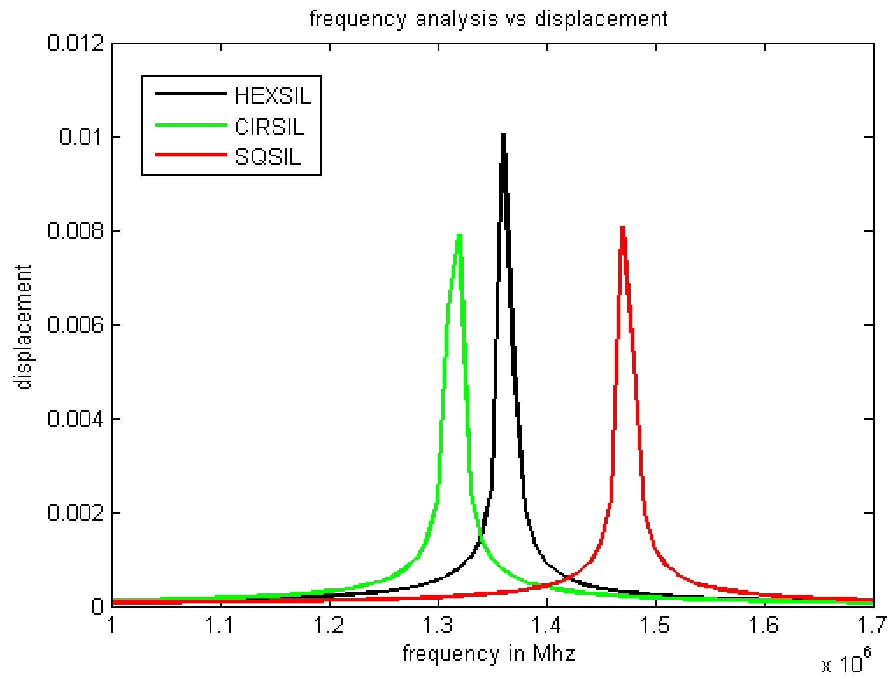

Fig. 6.4 Frequency versus deflection graph of three membranes

Figure 6.4 shows that if the area and thickness of the membranes are kept constant and silicon is selected as a membrane material then deflection is 0.1 μm for hexagonal membrane at Eigen frequency of 1.36 MHz, and deflection is 0.08 μm for circular membrane at Eigen frequency of 1.31 MHz. In case of square membrane, the deflection is 0.083 μm at the Eigen frequency of 1.41 MHz. In other words, for the same area and same material, deflection is lesser for square membrane and in order to obtain this deflection, it requires a higher frequency as compared to other membranes. Though circular membrane produces nearly the same deflection at a lower frequency.

Also, we can conclude that hexagonal membrane shows maximum deflection at a frequency of 1.36 MHz which is lower than square membrane but in close approximation with the circular membrane having frequency 1.31MHz. On the basis of these results, we simulated the hexagonal membrane for the three materials: the silicon, silicon nitride and polysilicon and the results of simulation are shown in fig. 6.5.

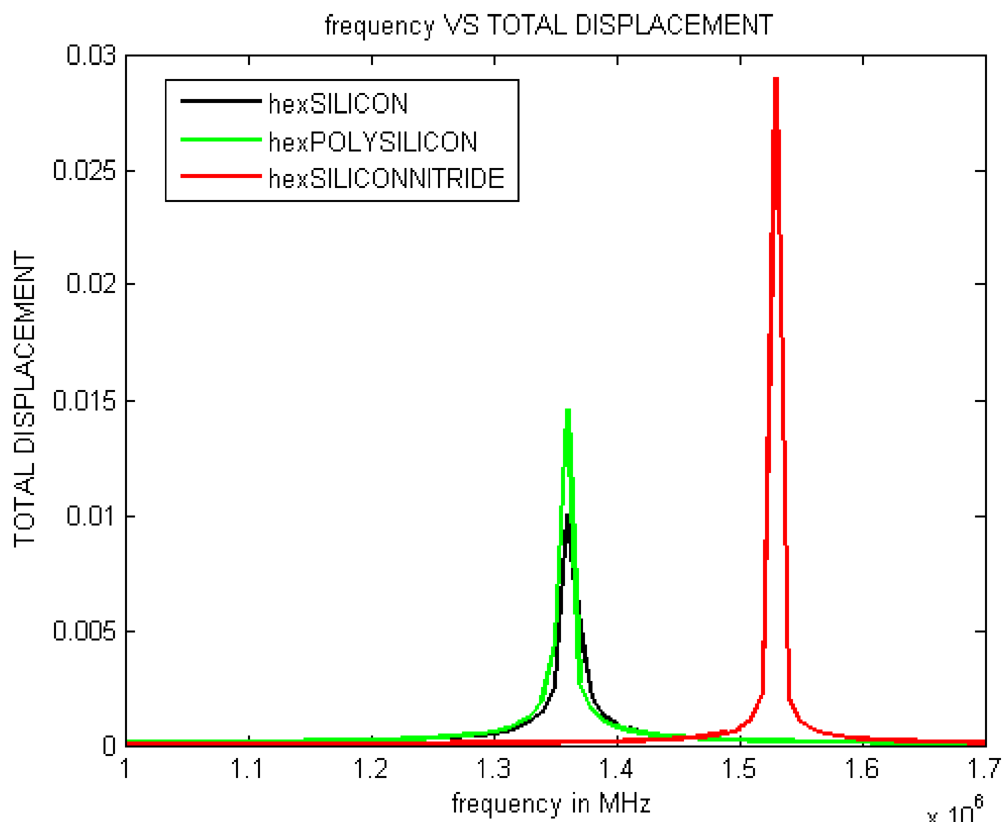

Fig. 6.5 Frequency versus deflection graph of hexagonal membrane using silicon, silicon nitride and polysilicon

Fig 6.5 shows that when hexagonal membrane is simulated with silicon, silicon nitride and polysilicon, the deflection observed is maximum in case of silicon nitride because

mechanical properties of silicon nitride membrane are better than those of silicon and polysilicon material.

6.3 DEFLECTION OF MEMBRANES UNDER DC BIAS VOLTAGE

This section explains the deflection of geometries under the effect of dc bias voltage. Deflection of geometries are calculated under various conditions such as air and water.

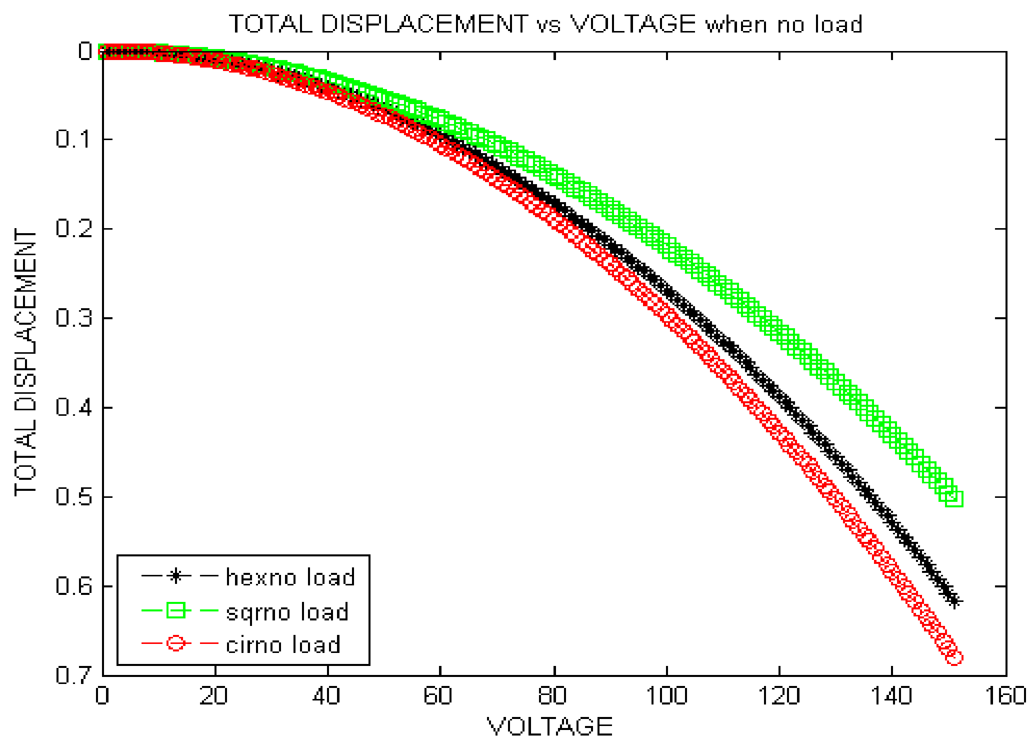

Fig. 6.6 Total displacement versus voltage graph when no load is applied on transducer

Fig. 6.6 shows the graph between deflection and DC voltage when no load is applied to the transducer. The use of DC voltage is already explained in the working principle of CMUT (chapter-3). The deflection is calculated for the range of 0-150V of DC. At 0 V, the deflection is zero because no force, neither mechanical nor electrical is acting on the transducer. The deflection is 1/3rd of the gap between the electrodes at 100 V for circular geometry, at 105V for hexagonal geometry and at 116V for the square geometry. Thus as expected, bias voltage is lower for circular geometry as compared to the other two geometries. But hexagonal geometry causes the same deflection at 105V which is closer in approximation with the circular geometry, so it can be used as alternative to circular geometry.

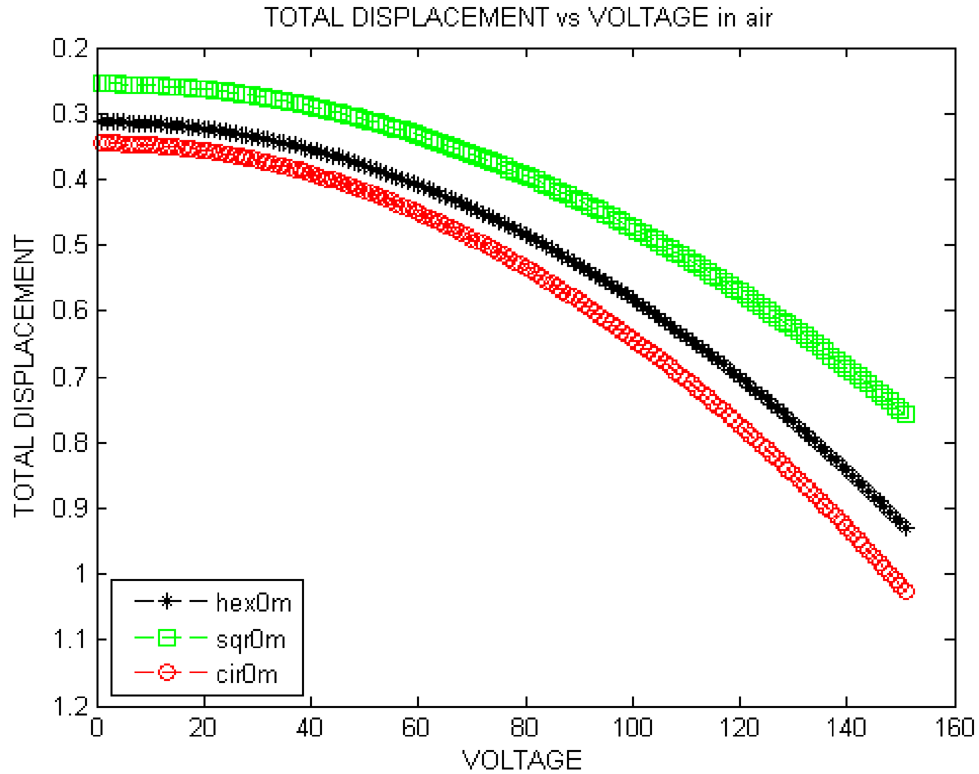

Fig. 6.7 Total displacement versus voltage graph under the effect of 1atm pressure

Fig 6.7 illustrates the results of displacement versus DC voltage when transducer is placed in air. In this case, pressure of 1 atm acts on the membrane. At 0 V, the deflection of membrane is observed as 0.34 µm in case of circular geometry, 0.31 µm for hexagonal geometry and 0.25 µm for square geometry. Here, CMUT operates in collapse mode as expected and is able to generate and detect ultrasound more effectively than a CMUT operating in conventional mode. The depth versus pressure table is shown below in table 6.3.

Table 6.3 Table of depth versus pressure

Depth(in metres)	**Pressure(atm)**	**Force (N/m^2)**
0	1	101325.00
1	1.09920	111376.44
2	1.19841	121428.89
3	1.29761	131480.33
4	1.39681	141531.77
5	1.49602	151584.22
6	1.59522	161635.66
7	1.69443	171688.11
8	1.79363	181739.55
9	1.89283	191790.99
10	1.99204	201843.45

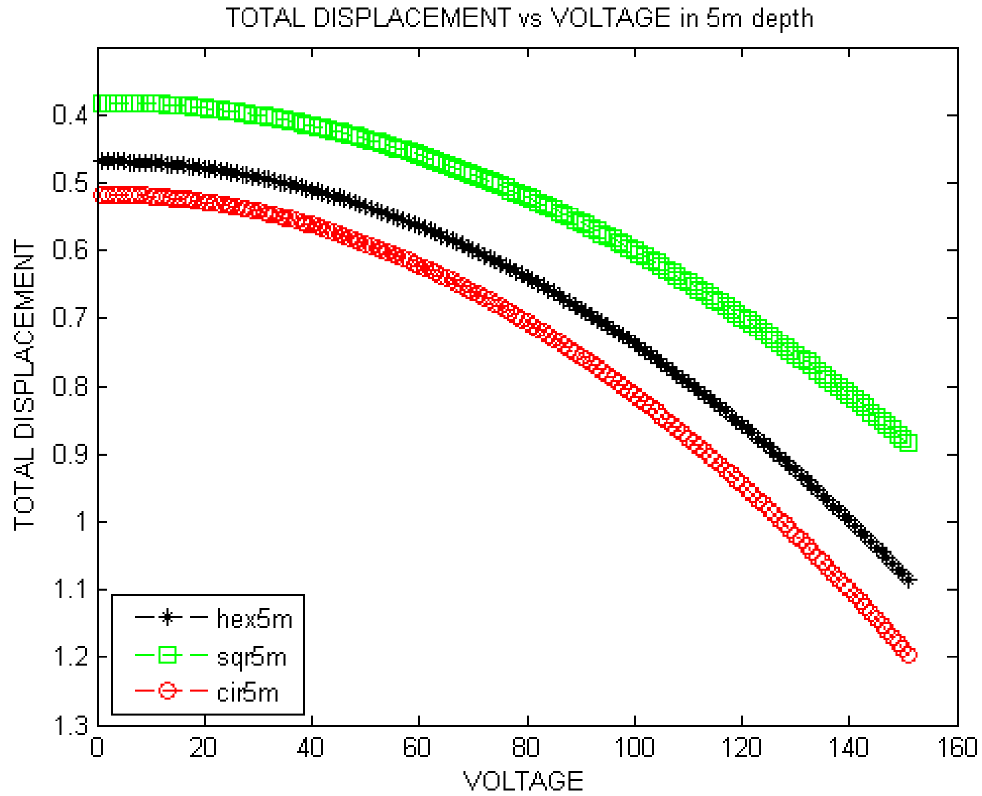

Fig. 6.8 Total displacement versus voltage graph under the effect of water

Fig 6.8 illustrates the results of displacement versus DC voltage when the transducer is placed in water at a depth of 5 m. At zero volt, the observed deflection is 0.51 μm in case of circular geometry, 0.46 μm in hexagonal geometry and 0.38 μm in square geometry. Thus, we observed that the deflection for the discussed cases is highest for circular geometry. Although, hexagonal geometry is also in close approximation to this. Thus, we have discussed hexagonal and circular geometry in detail and neglected the square geometry in further section. Table 6.4 lists the values parameters used for simulation of CMUT.

Table 6.4 List of parameters of CMUT

Parameter name	Value	Description
Sub	56.4[μm]	Width of substrate
Hsub	5[μm]	Thickness of substrate
Hisol	0.2[μm]	Thickness of insulating layer
Hgap	1[μm]	Height of cavity
Reltop	46.4[μm]	Radius of top electrode
Hmem	1[μm]	Thickness of membrane
heltop	0.2[μm]	Thickness of top electrode
Freq	2[MHz]	Excitation frequency
Vdc	80[V]	Applied dc voltage
Volt	10[V]	Applied ac voltage

The simulated Capacitive Micromachined Ultrasonic Transducer is shown in fig. 6.9.

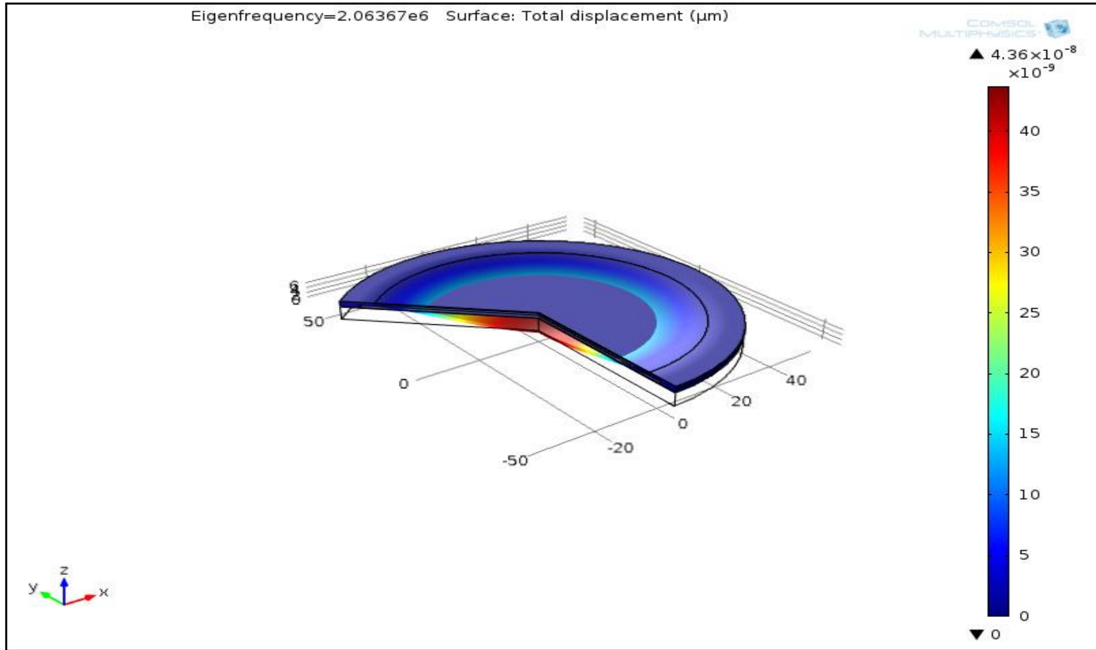

Fig. 6.9 Simulated Capacitive Micromachined Ultrasonic Transducer

Electrostatic and solid mechanics physics are coupled for this simulation. Electrostatic forces on the membrane are calculated in the electrostatic interface and defined in the solid mechanics interface. Following equations are used for the simulations [44]. The surface charge equals the norm of the electric displacement as:

$$\sigma = \varepsilon \mathrm{E} = \mathrm{D} \tag{6.2}$$

f is the force per unit area originated from the pull of the electric field in the induced charge is:

$$\mathrm{f} = \sigma \mathrm{E} = \varepsilon \mathrm{E}^2 = \mathrm{D.E} \tag{6.3}$$

The components of f can be written as:

$$\mathrm{f_x} = \mathrm{E_x}.\,|\mathrm{D}| \qquad (6.4)$$

$$\mathrm{f_y} = \mathrm{E_y}.\,|\mathrm{D}| \qquad (6.4)$$

Here E_x and E_y are the components of the electric field and $|D|$ is the norm of electric displacement. For this simulation, the mesh is resized and maximum size of mesh elements is selected to be 0.06 µm and the Eigen frequency is calculated to be 2.06

MHz. This model is simulated under 2D symmetric axis model builder for the sake of simplicity and sector angle is selected to be 255 degrees.

The Eigen frequency calculated from the above simulation result (fig. 6.9) is approximately 2 MHz and as CMUT converts the electrical signal into ultrasound and vice-versa, so high frequency signal is transmitted through membrane therefore an AC signal of frequency 2 MHz is applied to the transducer. Simulated data is shown in the table 6.5.

In the fig. 6.10, ultrasound wave of 2MHz is produced by the CMUT. Time evolution tracks that simulation has been performed as expected. When we used CMUT for underwater aucoustig imgaing, the eigen frequency will decrease as the pressure exerted by the water on membrane. As we discussed earlier, mechanical and elecrostaitc forces are acting on the CMUT. So the resonace frequency will be affected. The effect of electrostatic forces on the resonance frequency is shown in the fig. 6.11.

Fig. 6.10 Transient response of CMUT at 2MHz

Table 6.5 Table of simulated data for CMUT

% Model:	SIMULATED cmut.mph	
% Version:	COMSOL 4.4.0.150	
% Date:	May 20 2015, 12:18	
% Table:	Accumulated Probe Table 2 -	
% freq:	Time	1, Boundary Probe 2
2000000	0	1.00E-06
2000000	5.00E-09	1.00E-06
2000000	1.00E-08	9.99E-07
2000000	1.50E-08	9.99E-07
2000000	2.00E-08	9.98E-07
2000000	2.50E-08	9.97E-07
2000000	3.00E-08	9.95E-07
2000000	3.50E-08	9.93E-07
2000000	4.00E-08	9.91E-07
2000000	4.50E-08	9.89E-07
2000000	5.00E-08	9.86E-07
2000000	5.50E-08	9.82E-07
2000000	6.00E-08	9.78E-07
2000000	6.50E-08	9.74E-07
2000000	7.00E-08	9.69E-07
2000000	7.50E-08	9.64E-07
2000000	8.00E-08	9.58E-07
2000000	8.50E-08	9.52E-07
2000000	9.00E-08	9.45E-07
2000000	9.50E-08	9.38E-07
2000000	1.00E-07	9.32E-07
2000000	1.05E-07	9.25E-07
2000000	1.10E-07	9.18E-07
2000000	1.15E-07	9.11E-07
2000000	1.20E-07	9.04E-07
2000000	1.25E-07	8.98E-07
2000000	1.30E-07	8.91E-07
2000000	1.35E-07	8.85E-07
2000000	1.40E-07	8.79E-07
2000000	1.45E-07	8.73E-07
2000000	1.50E-07	8.67E-07
2000000	1.55E-07	8.61E-07
2000000	1.60E-07	8.56E-07
2000000	1.65E-07	8.50E-07
2000000	1.70E-07	8.45E-07
2000000	1.75E-07	8.41E-07
2000000	1.80E-07	8.36E-07
2000000	1.85E-07	8.32E-07
2000000	1.90E-07	8.28E-07
2000000	1.95E-07	8.24E-07

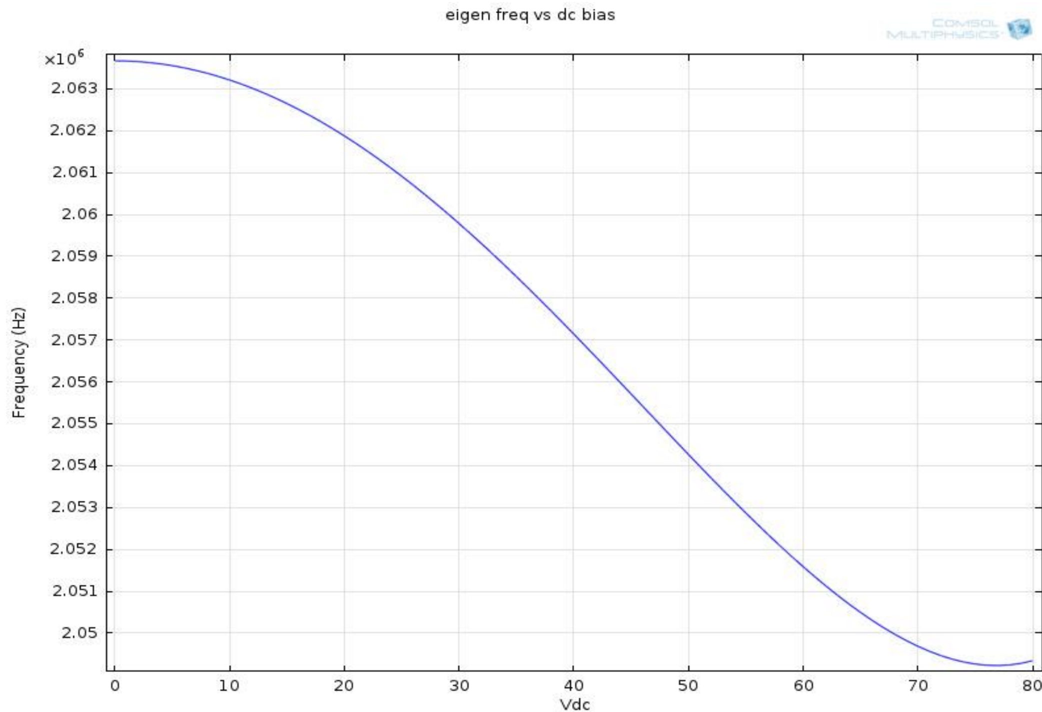

Figure 6.11 Eigen frequency versus DC bias

Hexagonal geometry: We designed hexagonal geometry for effective area of utilization as discussed earlier. Recalling the eigen frequency results, eigen frequency for circular membrane using silicon was 1.31 MHz and for hexagonal membrane, it was 1.36 MHz. These frequencis are calculated by using the same mesh and the same parameters. Also, it is strictly mentioned that eigen frequency can be changed by changing the mesh structure. Although this change is negligible. In COMSOL, according to geometry complexity, mesh should be refined otherwise it may lead to unexpected error. This error may occur because of small size of mesh elements near the edges and boundaries and because of narrow regions, although user can contol the mesh size according to the design. But it causes complexity in the compution and sometimes convergence of the solution becomes difficult. There are some feature in the tool like mapped mesh, edge, and free triangular which are available for resizing the mesh. The simulation of hexagonal CMUT following is carried out and the result is shown in fig. 6.12. Here, we will discuss the receiver side of hexagonal CMUT.

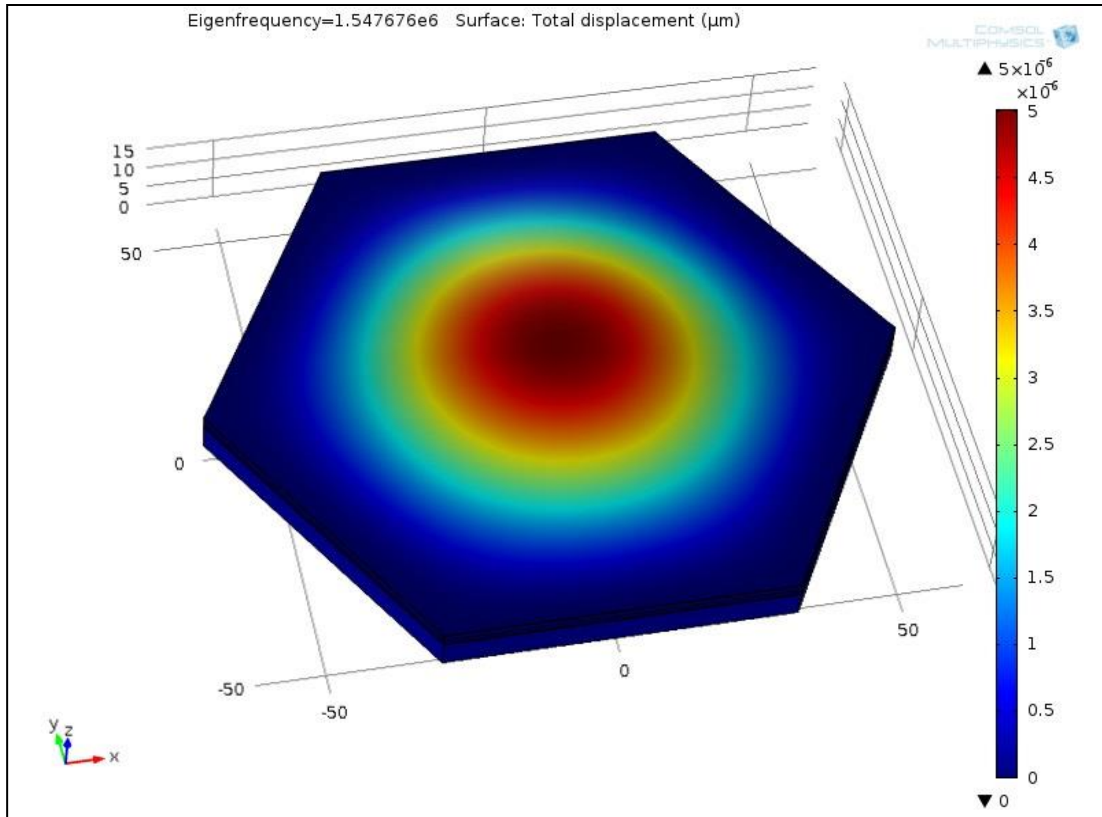

Fig. 6.12 Simulated hexagonal CMUT

Table 6.6 Parameters for hexagonal CMUT

Parameter name	Value	Description
Hsub	5 [µm]	Thickness of substrate
Hgap	1 [µm]	Thickness of cavity
Hmem	1 [µm]	Thickness of membrane
Heltop	0.2 [µm]	Thickness of top electrode
Vdc	80 [V]	DC voltage applied

In fig. 6.13 the top electrode shape is not completely hexagonal. This is because when we used CMUT in an array configuration, we need to connect different CMUT cells and for this purpose, we used metallization. Thus, in order to make contact; the shape is selected as shown in fig. 6.13. We can neglect the isolated layer in this case because we are using a 3D model for this case and electrode is at the top of the membrane. Also, the area covered by top electrode also an important factor, the defection is calculated for the different areas and this is shown in fig. 6.14.

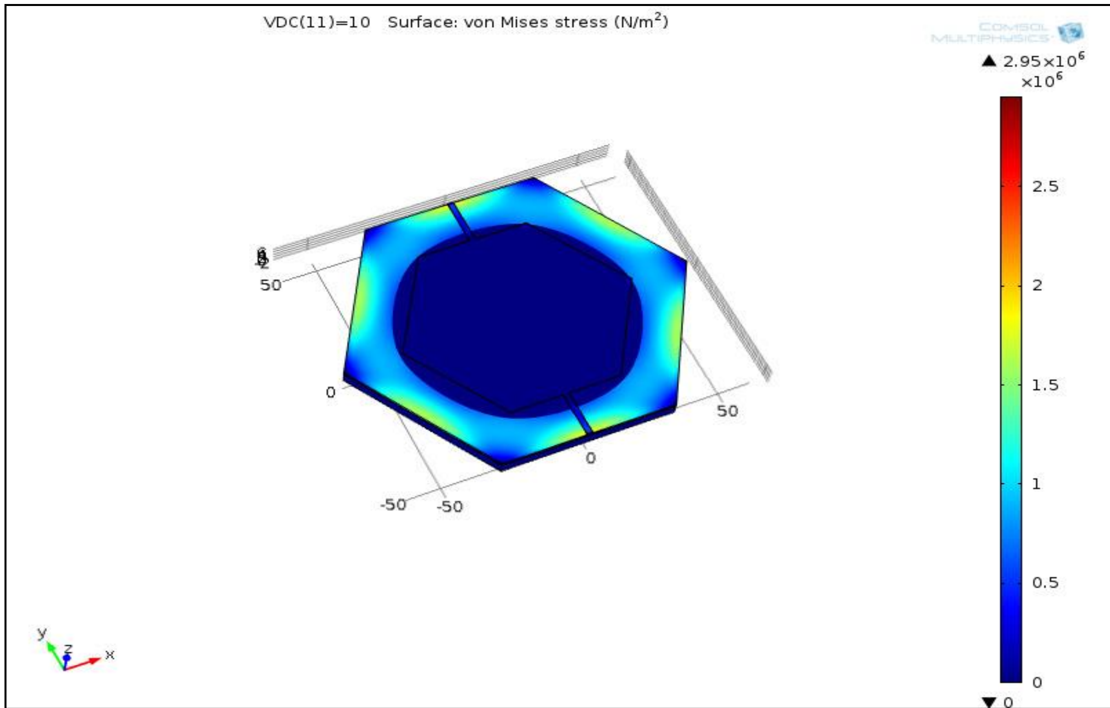

Fig. 6.13 Effect of top electrode

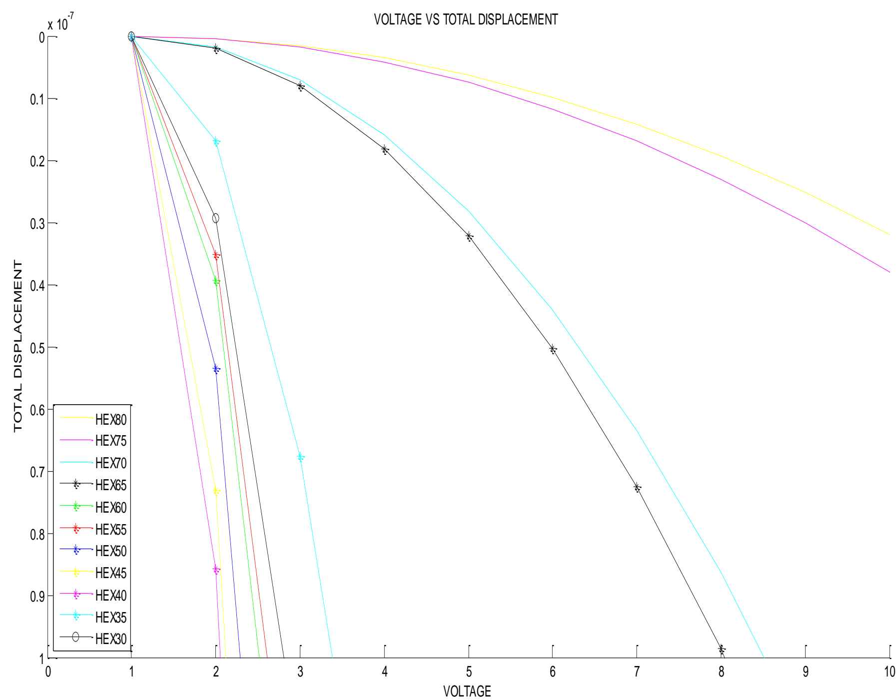

Fig. 6.14 Effect of area on top electrode

Form the above results; we can see that the 40 percent area of top electrode having thickness 0.2 µm causes the maximum deflection. For area greater than 40 percent the

deflection starts decreasing. The change in capacitance is also given by according to the well known equation:

$$C = \frac{\varepsilon.A}{d} \tag{6.6}$$

where, ε (absolute permittivity) $=\varepsilon_0 \varepsilon_r$

$$\varepsilon_0 = 8.854 \times 10^{-12}\ \mathrm{F/m}$$

Relative permittivity of silicon nitride (ε) $= 5.47$

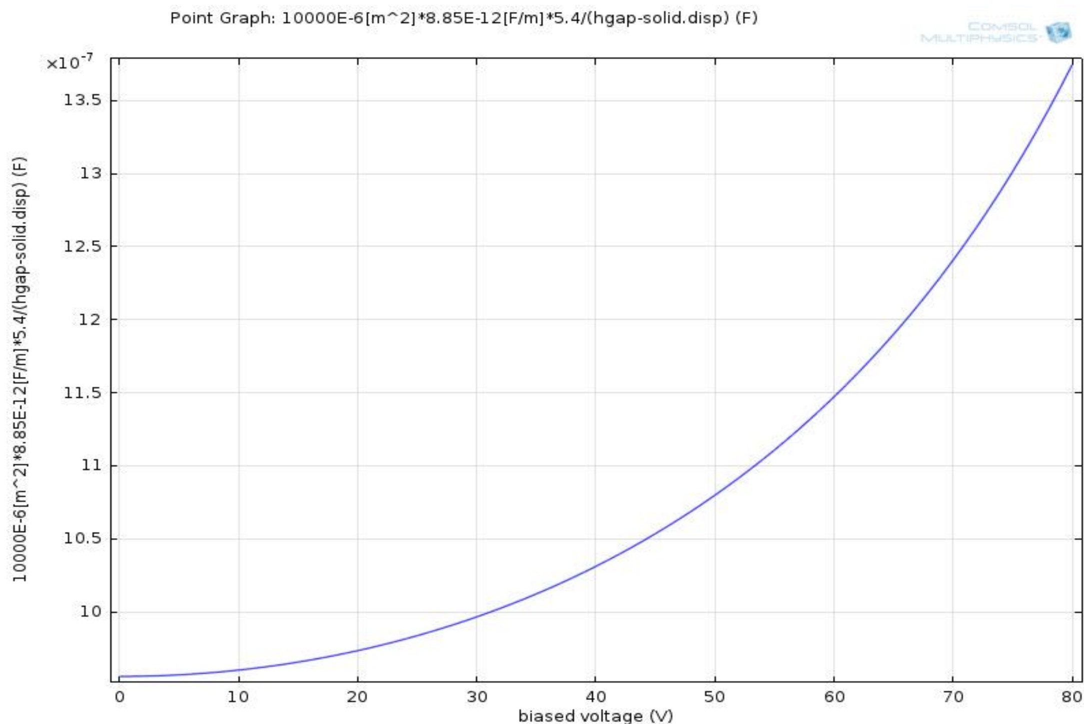

Fig. 6.15 Change in capacitance

The capacitance change with the biased voltage is shown graphically in fig. 6.15.

Conclusion: Thus from the above results we concluded that deflection in case of hexagonal CMUT is close approximation to circular CMUT under all the cases discussed above and also the area of top electrode is plays an important role in metallization process. On the basis of the above results, we can say that design parameters *i.e.,* thickness of cavity, thickness of membrane, thickness of electrode and pull-in voltage etc; of CMUT can change depending upon the application. Thus, these must be chosen according to the kind of application.

CHAPTER 7

CONCLUSION, RECOMMENDATIONS AND FUTURE SCOPE

1. From the above simulation results, we can see that performance of circular CMUT is best in terms of eigen frequency, pull in voltage and in maximum deflection as a function of DC bias. But for array formation the results are not satisfactory because of voids, so area is not effectively utilized. So we can use hexagonal geometry for effective utilization of area.

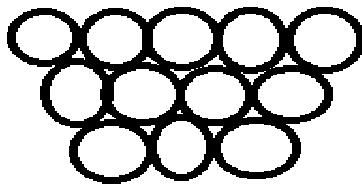

Fig. 7.1 Circular close packing

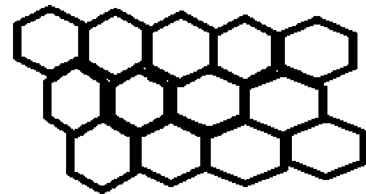

Fig.7.2 Hexagonal close packing

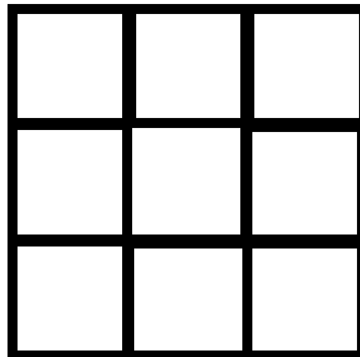

Fig. 7.3 Square close packing

2. Hexagonal geometry is discussed above and simulated for the dc bias voltage and as from the working principle of CMUT, we know that dc voltage is required when CMUT is used as receiver. Therefore, ac analysis is required to be done when it is used as transmitter.

3. In this thesis work, we simulated single cell of CMUT and compared the results of simulation. Analytical modeling needs to be done for verification of these results. Analysis of capacitive micro machined ultrasonic transducer has to be carried out for various parameters namely collapse voltage, resonance frequency, capacitance

changed and membrane geometry. An optimized design of CMUT will be established which can be further fabricated.

4. In future, simulation of CMUT arrays configuration need to be done and further work can be carried out to find appropriate spacing and dimensions for array elements which may lead to high resolution imaging with less complexity in design and give better images. A relatively new concept beam steering can be employed after forming the array.

5. To achieve various parameters namely thickness of membrane, cavity thickness for high resolution images so as to maximize the efficiency of the device.

6. New materials having the better mechanical and electrical properties can be considered for the membranes.

REFERENCES

[1] M. Mehregany, "Microelectromechanical system," *Circuit and Devices Magazine IEEE,* vol. 9, no. 6, pp. 14-22, 1993.

[2] H. J. Lee, K. K. Park, M. Kupnik and B. T. Khuri-Yakub, "Functionalization layers for CO2 sensing using capacitive Micromachined ultrasonic transducers," *Sensors and Actuators B: Chemical*, vol. 174, no. 1, pp. 87-93, 2012.

[3] J. Khandurina and A. Guttman, "Bio-analysis in microfluidic devices," *Journal of Chromatography A,* vol. 943, no. 2, pp. 159-183, 2002.

[4] S. D. Santhria, Microsystem design, London: Springer, 2004.

[5] W. Kuhl, G. R. Schodder and F. K. Schroder, "Condensor transmitters and microphones with solid dielectric for airborne ultrasonics," *Acoustica,* vol. 4, no. 5, pp. 519-532, 1954.

[6] D. W. Schindel and D. A. Hutchins, "Through-thickness characterization of solids by wideband air-coupled ultrasound," *Ultrasonics,* vol. 33, no. 1, pp. 11-17, 1995.

[7] D. W. Schindel, D. A. Hutchins and W. A. Grandia, "Capacitive and piezoelectric air-coupled transducers for resonant ultrasonic inspection," *Ultrasonics,* vol. 34, no. 6, pp. 621-627, 1996.

[8] X. Jin and I. Labadum, "Fabrication and characterization of surface micromachined capacitive ultrasonic immersion transducers," *IEEE Journal of microelectromechanical systems,* vol. 8, no. 1, pp. 100-113, 1999.

[9] O. Oralkan, X. Jin, F. L. Degertekin and B. T. Khuri-Yakub "Simulation and experimental characterization of surface micromachined capacitive Ultrasonic transducer array element," *IEEE Transactions on Ultrasonics, Ferroelectrics and Frequency control,* vol. 46, no. 6, pp. 1337-1340, 1999.

[10] T. H. Gan, "The use of broadband Acoustic transducers and pulse compression techniques for air coupled ultrasonic imaging," *Ultrasonics,* vol. 39, no.1, pp. 181-194, 2001.

[11] M. Wilm, A. Reinhardt, V. Laude, R. Armati, W. Daniau and S. Ballandras, "Three-dimensional modelling of Micromachined-ultrasonic-transducer arrays operating in water," *Science Direct Journal on Ultrasonics,* vol. 53, no. 1, pp. 457-465, 2004.

[12] B. Bayram, O. Oralkan, A. S. Ergun and B. T. Khuri-Yakub, "Capacitive micromachined ultrasonic transducer design for high power transmission," *IEEE Transactions on Ultrasonics, Ferroelectrics and Frequency Control,* vol. 52, no. 2, pp. 326-338, 2005.

[13] A. S. Ergun, Y. Huang, O. Oralkan and B. T. Khuri-Yakub, "Capacitive micromachined ultrasonic transducers: fabrication technology," *IEEE Transactions on Ultrasonics, Ferroelectrics and Frequency Control,* vol. 52, no. 12, pp. 2242-2258, 2005.

[14] I. Cicek, A. Bozkurt and M. Karaman, "Design of a front-end integrated circuit for 3D acoustic imaging using 2D CMUT arrays," *IEEE Transactions on Ultrasonics, Ferroelectrics and Freuency Control,* vol. 52, no. 12, pp. 2235-2241, 2005.

[15] A. Caronti, G. Caliano, R. Carotenuto, A. Savoia, M. Papparlardo, E. Cianci and V. Foglietti, "Capacitive micromachined ultrasonic transducer (CMUT) arrays for medical imaging," *Microelectronics Journal,* vol. 37, no. 8, pp. 770-777, 2006.

[16] J. Chen, X. Cheng, C. C. Chen, P. C. Li and Y. T. Cheng, "A capacitive micromachined ultrasonic transducer array for minimally invasive medical diagnosis," *Journal of Electromagnetic Systems,* vol. 17, no. 3, pp. 599-609, 2008.

[17] X. Cheng, J. Chen and C. Li, "A miniature CMUT array for minimally invasive photoacoustic imaging," *Journal of Electromechanical Systems,* vol. 19, no. 4,

pp. 1002-1011, 2010.

[18] D. S. Li, X. Zhaung, S. H. Vong, M. Kupnik and B. T. Khuri-Yakub, "Encapsulation of CMUT using viscoelastic polymer," *Journal of Electromechanical Systems,* vol. 19, no. 6, pp. 1341-1351, 2010.

[19] B. S. Cha, S.-M. Lee, T. Kanashima, M. Okuyama and T. Tanaka, "Influences of perforation ratio in characteristics of capacitive Micromachined ultrasonic transducers in air," *Sensors and Actuators A,* vol. 171, no. 1, pp. 191-198, 2011.

[20] A. O. Manzanares and F. M. de Espinosa, "Air-coupled MUMPs capacitive Micromachined ultrasonic transducers with resonant cavities," *Ultrasonics,* vol. 52, no. 1, pp. 482-489, 2012.

[21] A. C. J. W. Bhuyan, B. C. Leeand and B. T. Khuri-Yakub, "Integrated circuits for volumetric ultrasound imaging with 2-D CMUT arrays," *IEEE Transactions on Biomedical Circuits and Systems,* vol. 7, no. 6, pp. 796-804, 2013 .

[22] D. K. Kim, S. W. Chung, B. G. Jeong, S. W. Hong and H. Shin, "An indirectly clamped capacitive Micromachined ultrasonic transducer with a high electromechanical coupling factor," *Sensors and Actuators A,* vol. 203, no. 1, pp. 82-91, 2013.

[23] K. K. Park and B. Khuri-Yakub, "3-D airborne ultrasound synthetic aperture imaging based on capacitive Micromachined ultrasonic transducers," *Ultrasonics,* vol. 53, no. 7, pp. 1355-1362, 2013.

[24] A. Bybi, S. Grondel, J. Assaad, A.-C. Hladky-Hennion, C. Granger and M. Rguiti, "Reducing crosstalk in array structures by controlling the excitation voltages of individual elements: A feasibility study," *Ultrasonics,* vol. 53, no. 6, pp. 1135-1140, 2013.

[25] B.G. Jeong, "Performance and realibility of new CMUT design with improved efficiency," *Sensors and Actuators A: Physical,* vol. 199, no. 1, pp. 325-333, 2013.

[26] K. K. Park, O. Oralkan and B. T. Khuri-Yakub, "A comparison between conventional and collapse CMUT in 10 MHz 1-D array," *IEEE Transactions on Ultrasonics, Ferroelectrics and Frequency Control,* vol. 60, no. 6, pp. 1245-1255, 2013.

[27] L. L. P. Wong, A. I. H. Chen, Z. Li, A. S. Logan and J. T. W. Yeow, "A row-column addressed Micromachined ultrasonic transducer array for surface scanning applications," *Ultrasonics,* vol. 54, no. 8, pp. 2072-2080, 2014.

[28] A. Bybi, C. Granger, S. Grondel, A.-C. Hladky-Hennion and J. Assaad, "Electrical method for crosstalk cancellation in transducer arrays," *NDT & E International,* vol. 62, no. 1, pp. 115-121, 2014.

[29] M. L. Kuntzman, D. Kim and N. A. Hall, "Microfabrication and experimental evaluation of CMUT," *Journal of Electromechanical Systems,* vol. 24, no. 2, pp. 404-413, 2015.

[30] O. Oralkhan, A. S. Ergun, J. A. Johnson, M. Karaman, U. Demirci, K. Kaviani, T. H. Lee and B. T. Khuri-Yakub, "Capacitive micromachined ultrasonic transducers: next generation arrays for acoustic imaging?", *IEEE Transactions on Ultrasonics, Ferroelectrics and Frequency Control,* vol. 49, no. 11, pp. 1596-1610, 2002.

[31] A. Chhikara and S. Malik, "Parameters affecting the performance of capacitive Micromachined ultrasonic transducer," *International Journal of Applied Sciences and Engineering Research,* vol. 3, no. 2, pp. 333-338, 2014.

[32] I. Ladabaum, X. Jin, H. T. Soh, A. Atalar and B. T. Khuri-Yakub, "Surface micromachined capacitive ultrasonic transducer," *IEEE Transactions on Ultrasonics, Ferroelectrics and Frequency Control,* vol. 45, no. 3, pp. 67-690, 1998.

[33] I. Labadum, X. J. Hyongsok, T. Soh, A. Atalar and B. T. Khuri-Yakub, “Surface micromachined capacitive ultrasonic transducers,” *IEEE Transactions on Ultrasonics, Ferroelectrics and Frequency Control,* vol. 45, no. 3, pp. 678-689,

1998.

[34] I. J. Oppenheim, A. Jain and D. W. Greve, “MEMS ultrasonic transducers for the testing of solids” *IEEE Transactions on Ultrasonics, Ferroelectrics and Frequency Control,*vol. 50, no. 3, pp. 305-311, 2003.

[35] S. K. Tiwari, B. S. Satyanarayana, A. G. Pai and K. K. Trivedi, "Circular capacitance micromachined ultrasonic transducer," *Defence Science Journal,* vol. 59, no. 6, pp. 627-633, 2009.

[36] B. Bayram, E. Haeggstorm, G. Yaralioglu and B. T. Khuri-Yakub, "A new regime for operating capacitive Micromachined ultrasonic transducers," *IEEE Transactions on Ultrasonics, Ferroelectrics and Frequency Control,* vol. 30, no. 1, pp. 1184-1190, 2003.

[37] *Introduction to COMSOL Multiphysics Users Manual*, October, 2012.

[38] S. H. Wong, “Capacitive Micromachined Ultrasonic Transducers for Therapeutic Ultrasound” Ph. D. dissertation, Electrical Engg. Dept., Standford Univ., United States, 2008.

[39] Y. Huang, A. S. Ergun, E. Hæggstrom, M. H. Badi and B. T. Khuri-Yakub, “Fabricating capacitive micromachined ultrasonic transducers with wafer-bonding technique,” *IEEE Journal of Microelectromechanical Systems*, vol.12, no.2, pp. 128-137, 2003.

[40] P.C. Eccardt, K. Nierderer, T. Scheiter and C. Hierold, “Surface micromachined ultrasonic transducers in CMOS technology,” in *Proceedings of IEEE Ultrasonics Symposium*, vol. 2, no. 1, pp. 959-962, 1996.

[41] R. A. Noble, A. R. D. Jones, T. J. Robertson, D. A. Hutchins and D. R. Billson, “Novel, wide bandwidth, micromachined ultrasonic transducers,” *IEEE Transactions on Ultrasonics, Ferroelectrics and Frequency Control,* vol. 48, no. 6, pp. 1495-1507, 2001.

[42] J. Knight, J. M. Lean and F. L. Degertekin, “Low temperature fabrication of

immersion capacitive micromachined ultrasonic transducers on silicon and dielectric substrates,” *IEEE Transactions on Ultrasonics, Ferroelectrics and Frequency Control*, vol. 51, no. 10, pp. 1324-1333, 2004.

[43] P. R. Scheeper, W. Olthuis and P. Bergveld, “Fabrication of subminiature silicon condenser microphone using the sacrificial layer technique,” in proceedings of International Confrence on Transducers, San Francisco, 1991.

[44] F. F. D. Agnol and A. C. F. de Mattos, "Development of a micro ultrasonic transducer," in proceedings of COMSOL Confrence, Campinas, Brazil, 2014.

LIST OF PUBLICATIONS

[1] Vinod Bhonsle and Anil Arora, "Capacitive Micromachined Ultrasonic Transducer", in *Proceeding of National Conference on Advances in Electrical & Electronics Communication Engineering,(AEECE-15),* pp.1-3, Feb. 20-21, 2015.